Journal of Sound and Vibration 329 (2010) 371–393

Contents lists available at ScienceDirect

Journal of Sound and Vibration

journal homepage: www.elsevier.com/locate/jsvi

A dynamic model to predict modulation sidebands of a planetary gear set having manufacturing errors

Murat Inalpolat, Ahmet Kahraman *

Department of Mechanical Engineering, The Ohio State University, 201 W. 19th Ave., Columbus, OH 43210-1107, USA

ARTICLE INFO

Article history:
Received 2 June 2009
Received in revised form
15 September 2009
Accepted 16 September 2009
Handling Editor H. Ouyang
Available online 12 October 2009

ABSTRACT

In this study, a nonlinear time-varying dynamic model is proposed to predict modulation sidebands of planetary gear sets. This discrete dynamic model includes periodically time-varying gear mesh stiffnesses and the nonlinearities associated with tooth separations. The model uses forms of gear mesh interface excitations that are amplitude and frequency modulated due to a class of gear manufacturing errors to predict dynamic forces at all sun-planet and ring-planet gear meshes. The predicted gear mesh force spectra are shown to exhibit well-defined modulation sidebands at frequencies associated with the rotational speeds of gears relative to the planet carrier. This model is further combined with a previously developed model that accounts for amplitude modulations due to rotation of the carrier to predict acceleration spectra at a fixed position in the planetary transmission housing. Individual contributions of each gear error in the form of amplitude and frequency modulations are illustrated through an example analysis. Comparisons are made to measured spectra to demonstrate the capability of the model in predicting the sidebands of a planetary gear set with gear manufacturing errors and a rotating carrier.

1. Introduction

Vibration and noise spectra from planetary gearboxes and transmissions often exhibit components at distinct frequencies around the gear mesh (tooth passing) frequency and its higher harmonics. The origin of a subset of these *sideband* components was proposed to be associated with the rotation of the planet carrier that causes amplitude modulations of the dynamic forces of the gear meshes that rotate with the carrier [1–3]. A recent study by these authors provided an analytical framework for predicting the amplitude modulation sidebands of this kind [4]. This model showed that the amplitude modulations (AM) of an acceleration spectrum due to rotation of the carrier are defined by (i) the number of planets in the gear set, (ii) planet spacing angles around the sun gear, and (iii) number of teeth of gear components. These parameters that define relative phasing relationships among the planet meshes not only impact the force/vibration cancellation and neutralization schemes that are studied widely [5,6], but also define the frequencies and amplitudes of certain sidebands on vibration spectra. Based on their simplified model that assumes that the dynamic gear mesh forces are known up-front, Inalpolat and Kahraman [4] classified planetary gear sets based on their sideband behavior in five groups: (1) equally-spaced and in-phase planets, (2) equally-spaced and sequentially phased planets, (3) unequally-spaced and in-phase planets, (4) unequally-spaced and sequentially phased planets, and (5) unequally spaced

* Corresponding author. Tel.: +1 614 292 4678.
E-mail address: kahraman.1@osu.edu (A. Kahraman).

0022-460X/$ - see front matter © 2009 Elsevier Ltd. All rights reserved.
doi:10.1016/j.jsv.2009.09.022

and arbitrarily phased planets. They established rules for sidebands for each category to be produced by the rotation of the carrier. They also performed experiments with gear sets from different categories to verify these rules.

The measured acceleration spectra presented in Ref. [4] contained additional sideband activity that is not possible to describe solely by AM caused by the rotation of the carrier. The cause of these additional sidebands can be attributable to certain manufacturing errors of the gears. Chaari et al. [7] developed a discrete dynamic model of a planetary gear set to predict the influence of such errors in the form of gear run-out (eccentricity) on the dynamic gear mesh forces due to changes to the gear motion transmission error excitations. Another potential cause for planetary gear set sidebands was suggested to be the unequal planet load sharing that is mostly impacted by the errors of the planet carrier. In one such study, Mark and Hines [8] predicted the effect of unequal planet load sharing due to a crack on the carrier planet posts on the sideband distributions.

Most of the above studies focused on AM effects. Published studies on frequency modulations (FM) did not consider planetary gear sets [9–11]. They focused on analytical treatment of FM of a class of oscillators, which can be representative of a single gear pair. Randall [9], and Sweeney and Randall [10] qualitatively explained some of the possible sources of gear signal modulations for parallel-axis gears by performing simplified simulations. They presented possible effects of manufacturing errors on the resultant vibration spectra via amplitude and phase modulations. In another paper, Blankenship and Singh [11] studied both amplitude and angle modulations of a damped oscillator analytically and developed solution methodologies for the governing equations. Besides these studies, there are a variety of works that deal with sidebands in the wider context of planetary gear vibrations [12–19]. The same is true for studies on planetary vibration condition monitoring for diagnostics purposes [19–21].

This study aims at expanding on the previous work presented in Ref. [4] by (i) providing a nonlinear time-varying model of a planetary gear set to predict dynamic gear mesh forces, (ii) formulating modulated gear mesh stiffness and gear transmission error excitations due to certain gear manufacturing errors, and (iii) combining the dynamic model with the AM formulation proposed for carrier rotation [4]. This unified discrete dynamic model is intended to include both AM and FM due to gear manufacturing errors as well as AM due to the rotation of the carrier to seek a fundamental understanding of mechanisms of modulation sidebands in planetary gear sets. The model will be formulated in a general way to handle a planetary gear set with any number of planets that are spaced in any arbitrary positions such that all five categories of gear sets specified in Ref. [4] can be handled dynamically. The model will be used to simulate an example planetary gear set to study the individual contributions of amplitude and frequency modulations due to various errors and to arrive at rules in identifying them on a given vibration or noise spectrum. At the end, the model predictions will be compared with a measured vibration spectrum from a planetary gearbox to demonstrate the effectiveness of the model in predicting sidebands of a planetary gear set.

The influences of unequal planet load sharing [22] as well as elastic deformations of gear bodies on modulation sidebands will not be included in this study and the flexibilities will be kept limited to the gear meshes and radial bearings. The model will focus primarily on simple planetary gear sets (each planet meshing with the same sun and ring gears). However, the same methodology can be applied to other kinematic forms of planetary gear sets such as double-planet gear sets, compound (multistage) planetary gear sets and complex-compound planetary gear sets [23,24]. In a recent study, certain operating conditions such as fluctuation of the input torque to the planetary gear set were stated to cause additional sidebands [25,26]. This study focuses only on the sideband behavior at steady-state operating conditions. Any additional modulations due to time-varying speed or torque were not included in this study, with the premise that a steady-state baseline must be established before recognizing signs of these added complexities on the vibration spectra.

2. Prediction of modulation sidebands under dynamic conditions

The modeling methodology employed here consists of two major steps. The first step is to predict the dynamic gear mesh forces by using a discrete dynamic model that includes various forms of typical manufacturing errors. As these errors modulate the excitations used for the dynamic model, the predicted dynamic mesh force spectra should be expected to contain sideband orders associated with these errors. In case of a gear set with a stationary carrier, the measured vibration spectra on the housing as well as the noise around the gearbox will have the same spectral characteristics as the dynamic mesh forces. However, when the planet carrier rotates, planets move with it relative to any fixed measurement location, causing additional amplitude modulations [4]. Accordingly, the second step in this methodology is to apply the amplitude modulation formulation of Ref. [4] to the dynamic gear mesh forces predicted by the dynamic model to capture the combined influence of manufacturing errors and carrier rotation on the modulation sidebands of the planetary gear sets.

2.1. Dynamic model of planetary gear set

A discrete, two-dimensional time-varying dynamic model is considered here. This model is based on an earlier model [27] that was developed to study planet load sharing characteristics of a simple planetary gear set under dynamic conditions. This model will be expanded here to include the influences of various gear and carrier related manufacturing errors. The model considers a simple planetary gear set with N planets (typically N=3–7 for most automotive and aerospace applications) that are positioned in any angular spacing allowed by the geometric constraints. As N and the spacing angles

of planets ψ_i, ($i \in [1,N]$ with $\psi_1=0$) together with the number of teeth of gears were shown to define amplitude modulations due to carrier rotation [4], it is essential that the dynamic model should have the capability to model a gear set with any combinations of the same parameters.

The dynamic model of the planetary gear set shown in Fig. 1 allows each gear and carrier body j to translate in x and y directions, denoted by x_j and y_j, and rotate about its axis that remains normal to the transverse plane of the gears. The fluctuations of the same member about its nominal rigid-body rotation are defined by θ_j. Each planet (pi) is in mesh with the sun gear (s) and the ring (internal) gear (r) while it is supported through its axis by a bearing held by the carrier (c). In Fig. 1, only one of the N planet branches located at an arbitrary planet position angle ψ_i is shown. In this figure, $\overline{\theta}_{jc}$ (j=s,r,pi) are the nominal kinematic rotations and ε_j represents the initial position angle of the run-out (eccentricity) vector of each gear j. Here, ε_s and ε_r are both defined from the horizontal x-axis while ε_{pi} is defined from the radial axis along the centers of the sun gear (O) and planet pi located at an angle ψ_i.

A gear pair (external or internal) sub-system and a pinion–carrier pair sub-system, as shown in Fig. 2, will be formulated first before assembling the dynamic model of the entire gear set. Fig. 2(a) and (b) show dynamic models of external (sun-planet pi) and internal (ring-planet pi) gear pairs, respectively, with planet pi positioned at angle ψ_i. Gears are modeled as rigid disks with masses m_s, m_r and m_p, and mass moments of inertia J_s, J_r and J_p. The gear mesh interfaces are represented by (i) periodically time-varying gear mesh stiffnesses $k_{spi}(t)$ and $k_{rpi}(t)$ to account for the fluctuation of the stiffness with gear rotations [27], (ii) constant gear mesh damping elements c_{sp} and c_{rp} that are assumed to be the same for each s–pi and r–pi mesh, and (iii) periodic gear transmission error displacement excitations $e_{spi}(t)$ and $e_{rpi}(t)$ [27].

Defining $u_j=r_j\theta_j$ (j=s,r) and $u_{pi}=r_{pi}\theta_{pi}$ as the coordinates in place of θ_j and θ_{pi} where r_j and r_{pi} are the radii of the gears, and further defining the dynamic gear mesh forces as

$$F_{jpi}(t) = c_{jp}\dot{p}_{jpi}(t) + k_{jpi}(t)p_{jpi}(t), \tag{1a}$$

where $p_{jpi}(t)$ is the relative gear mesh displacement given as

$$p_{jpi}(t) = [y_j(t) - y_{pi}(t)]\cos\psi_{ji} - [x_j(t) - x_{pi}(t)]\sin\psi_{ji} - u_j(t) - \delta_j u_{pi}(t) - e_{jpi}(t) + E_{jpi}(t) - E_{pij}(t) \tag{1b}$$

equations of motion of a gear pair sub-system are written as

$$m_j\ddot{y}_j(t) + h_{jpi}\cos\psi_{ji}F_{jpi}(t) = 0, \tag{2a}$$

$$m_j\ddot{x}_j(t) - h_{jpi}\sin\psi_{ji}F_{jpi}(t) = 0, \tag{2b}$$

$$\frac{J_j}{r_j^2}\ddot{u}_j(t) - h_{jpi}F_{jpi}(t) = \frac{T_j}{Nr_j}, \tag{2c}$$

$$m_p\ddot{y}_{pi}(t) - h_{jpi}\cos\psi_{ji}F_{jpi}(t) = 0, \tag{2d}$$

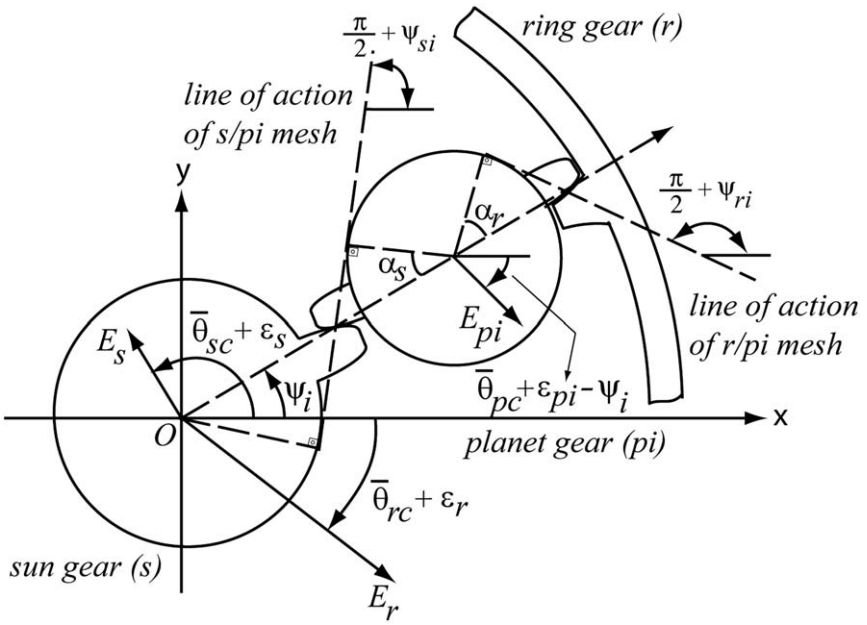

Fig. 1. Components and basic geometric parameters of a simple planetary gear set (only one planet branch is shown).

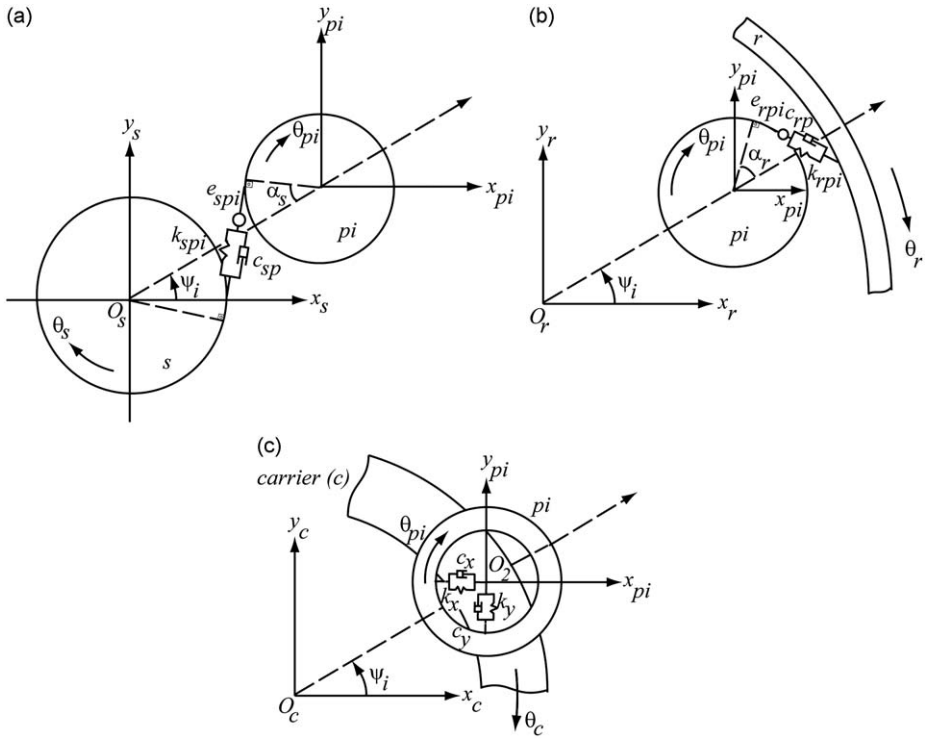

Fig. 2. Dynamic models of (a) a sun-planet *pi* pair, (b) a ring-planet *pi* pair, and (c) a carrier-planet *pi* pair.

$$m_p\ddot{x}_{pi}(t) + h_{jpi}\sin\psi_{ji}F_{jpi}(t) = 0, \tag{2e}$$

$$\frac{J_p}{r_p^2}\ddot{u}_{pi}(t) - \delta_j h_{jpi}F_{jpi}(t) = 0. \tag{2f}$$

In these equations, δ_j=1 for j=s (external s–pi gear pair) and δ_j=−1 for j=r (internal r–pi gear pair) and ψ_{ji}=ψ_i−$\delta_j\alpha_j$, as shown in Fig. 1, where α_j is the transverse pressure angle of the gears. The external torque T_j in Eq. (2c) represents the torque externally applied on the sun or the ring gear. An additional function h_{jpi} is applied as a multiplier to $F_{jpi}(t)$ to account for any nonlinear effects that might take place due to tooth separations. Here, h_{jpi}=1 when the gear teeth are in contact (i.e. $p_{jpi}(t)\geq 0$) and h_{jpi}=0 when gears loose contact (i.e. $p_{jpi}(t)<0$). Also included in Eqs. (1a) and (1b) are $E_{jpi}(t)$ and $E_{pij}(t)$ to represent manufacturing errors of gear j relative the planet pi and manufacturing errors of planet pi relative to gear j, respectively. These errors will be defined explicitly in the next section.

Eqs. (2a)–(2f) can be written in matrix form to obtain sub-matrices associated with the gear j-planet pi pair as

$$\mathbf{M}_{jpi} = \begin{bmatrix} \mathbf{m}_j & \mathbf{0} \\ \mathbf{0} & \mathbf{m}_{pi} \end{bmatrix}, \tag{3a}$$

$$\mathbf{C}_{jpi} = \begin{bmatrix} \mathbf{c}_{jpi}^{(11)} & \mathbf{c}_{jpi}^{(12)} \\ \mathbf{c}_{jpi}^{(12)} & \mathbf{c}_{jpi}^{(22)} \end{bmatrix}, \tag{3b}$$

$$\mathbf{K}_{jpi} = \begin{bmatrix} \mathbf{k}_{jpi}^{(11)} & \mathbf{k}_{jpi}^{(12)} \\ \mathbf{k}_{jpi}^{(12)} & \mathbf{k}_{jpi}^{(22)} \end{bmatrix} \tag{3c}$$

with displacement and force vectors

$$\mathbf{Q}_{jpi} = \begin{Bmatrix} \mathbf{q}_j \\ \mathbf{q}_{pi} \end{Bmatrix}, \tag{3d}$$

$$\overline{\mathbf{F}}_{jpi} = \begin{Bmatrix} \overline{\mathbf{f}}_j \\ \mathbf{0} \end{Bmatrix}, \tag{3e}$$

$$\mathbf{F}_{jpi}(t) = \begin{Bmatrix} \mathbf{f}_{jpi}^{(1)} \\ \mathbf{f}_{jpi}^{(2)} \end{Bmatrix}. \tag{3f}$$

Meanwhile, equations of motion for the carrier-planet *pi* sub-system, which is shown in Fig. 2(c) with $u_c = r_c\theta_c$ as the rotational carrier coordinate (r_c is the radius of the circle passing through the planet centers), are defined as

$$m_c\ddot{y}_c(t) + c_y[\dot{y}_c(t) - \dot{y}_{pi}(t) - \cos\psi_i\dot{u}_c(t)] + k_y[y_c(t) - y_{pi}(t) - \cos\psi_i u_c(t)] = 0, \tag{4a}$$

$$m_c\ddot{x}_c(t) + c_x[\dot{x}_c(t) - \dot{x}_{pi}(t) + \sin\psi_i\dot{u}_c(t)] + k_x[x_c(t) - x_{pi}(t) + \sin\psi_i u_c(t)] = 0, \tag{4b}$$

$$\begin{aligned} &\frac{J_c}{r_c^2}\ddot{u}_c(t) + c_x[\dot{x}_c(t) - \dot{x}_{pi}(t) + \sin\psi_i\dot{u}_c(t)]\sin\psi_i - c_y[\dot{y}_c(t) - \dot{y}_{pi}(t) - \cos\psi_i\dot{u}_c(t)]\cos\psi_i \\ &\quad + k_x[x_c(t) - x_{pi}(t) + \sin\psi_i u_c(t)]\sin\psi_i - k_y[y_c(t) - y_{pi}(t) - \cos\psi_i u_c(t)]\cos\psi_i \\ &\quad = \frac{T_c}{Nr_c}, \end{aligned} \tag{4c}$$

$$m_p\ddot{y}_{pi}(t) - c_y[\dot{y}_c(t) - \dot{y}_{pi}(t) - \cos\psi_i\dot{u}_c(t)] - k_y[y_c(t) - y_{pi}(t) - \cos\psi_i u_c(t)] = 0, \tag{4d}$$

$$m_p\ddot{x}_{pi}(t) - c_x[\dot{x}_c(t) - \dot{x}_{pi}(t) + \sin\psi_i\dot{u}_c(t)] - k_x[x_c(t) - x_{pi}(t) + \sin\psi_i u_c(t)] = 0. \tag{4e}$$

Here, T_c is the external torque applied to the carrier, and m_c and J_c are the mass and the polar mass moment of inertia of the carrier, respectively. In this model, the planet pin-bearing assembly is represented by linear springs k_x and k_y, and dampers c_x and c_y as illustrated in Fig. 2(c). It is noted that above equations are not a function of planet rotation $u_{pi} = r_p\theta_{pi}$ since planet *pi* can rotate freely relative to the carrier. Eqs. (4a)–(4e) are written in matrix form to define

$$\mathbf{M}_{cpi} = \begin{bmatrix} \mathbf{m}_c & \mathbf{0} \\ \mathbf{0} & \mathbf{m}_{pi} \end{bmatrix}, \tag{5a}$$

$$\mathbf{C}_{pi} = \begin{bmatrix} \mathbf{c}_{cpi}^{(11)} & \mathbf{c}_{cpi}^{(12)} \\ \mathbf{c}_{cpi}^{(12)} & \mathbf{c}_{cpi}^{(22)} \end{bmatrix}, \tag{5b}$$

$$\mathbf{K}_{cpi} = \begin{bmatrix} \mathbf{k}_{cpi}^{(11)} & \mathbf{k}_{cpi}^{(12)} \\ \mathbf{k}_{cpi}^{(12)} & \mathbf{k}_{cpi}^{(22)} \end{bmatrix}, \tag{5c}$$

$$\mathbf{Q}_{cpi} = \begin{Bmatrix} \mathbf{q}_c \\ \mathbf{q}_{pi} \end{Bmatrix}, \tag{5d}$$

$$\overline{\mathbf{F}}_{cpi} = \begin{Bmatrix} \overline{\mathbf{f}}_c \\ \mathbf{0} \end{Bmatrix}. \tag{5e}$$

With the matrices of every sub-system available, the overall equations of motion of an *N*-planet planetary gear set with planets spaced at ψ_i ($i \in [1,N]$) are constructed systematically as

$$\mathbf{M}\ddot{\mathbf{Q}}(t) + [\mathbf{C} + \mathbf{C}_b]\dot{\mathbf{Q}}(t) + [\mathbf{K}(t) + \mathbf{K}_b]\mathbf{Q}(t) = \overline{\mathbf{F}} + \mathbf{F}(t), \tag{6a}$$

where

$$\mathbf{Q} = \begin{bmatrix} \mathbf{q}_c & \mathbf{q}_r & \mathbf{q}_s & \mathbf{q}_{p1}, & \cdots & , \mathbf{q}_{pN} \end{bmatrix}^T, \tag{6b}$$

$$\mathbf{M} = \mathrm{Diag}\begin{bmatrix} \mathbf{M}_c & \mathbf{M}_r & \mathbf{M}_s & \mathbf{M}_{p1}, & \cdots & , \mathbf{M}_{pN} \end{bmatrix}, \tag{6c}$$

$$\mathbf{C} = \begin{bmatrix} \sum_{i=1}^{N}\mathbf{c}_{cpi}^{(11)} & 0 & 0 & \mathbf{c}_{cp1}^{(12)} & \cdots & \mathbf{c}_{cpN}^{(12)} \\ & \sum_{i=1}^{N}\mathbf{c}_{rpi}^{(11)} & 0 & -\mathbf{c}_{rp1}^{(12)} & \cdots & -\mathbf{c}_{rpN}^{(12)} \\ & & \sum_{i=1}^{N}\mathbf{c}_{spi}^{(11)} & \mathbf{c}_{sp1}^{(12)} & \cdots & \mathbf{c}_{spN}^{(12)} \\ & & & \mathbf{c}_{cp1}^{(22)} + \mathbf{c}_{rp1}^{(22)} + \mathbf{c}_{sp1}^{(22)} & \cdots & 0 \\ & & & & \ddots & \vdots \\ \text{symmetric} & & & & & \mathbf{c}_{cpN}^{(22)} + \mathbf{c}_{rpN}^{(22)} + \mathbf{c}_{spN}^{(22)} \end{bmatrix}, \tag{6d}$$

$$\mathbf{K}(t)=\begin{bmatrix} \sum_{i=1}^{N}\mathbf{k}_{cpi}^{(11)} & \mathbf{0} & \mathbf{0} & \mathbf{k}_{cp1}^{(12)} & \cdots & \mathbf{k}_{cpN}^{(12)} \\ & \sum_{i=1}^{N}\mathbf{k}_{rpi}^{(11)} & 0 & -\mathbf{k}_{rp1}^{(12)} & \cdots & -\mathbf{k}_{rpN}^{(12)} \\ & & \sum_{i=1}^{N}\mathbf{k}_{spi}^{(11)} & \mathbf{k}_{sp1}^{(12)} & \cdots & \mathbf{k}_{spN}^{(12)} \\ & & & \mathbf{k}_{cp1}^{(22)}+\mathbf{k}_{rp1}^{(22)}+\mathbf{k}_{sp1}^{(22)} & \cdots & 0 \\ & & & & \ddots & \vdots \\ \text{symmetric} & & & & & \mathbf{k}_{cpN}^{(22)}+\mathbf{k}_{rpN}^{(22)}+\mathbf{k}_{spN}^{(22)} \end{bmatrix}. \tag{6e}$$

In Eq. (6e), the elements of $\mathbf{K}(t)$ are periodically time-varying due to the mesh stiffnesses $k_{spi}(t)$ and $k_{rpi}(t)$ ($i\in[1,N]$).

The $\mathbf{C}_b$ and $\mathbf{K}_b$ matrices in Eq. (6a) represent the bearing damping and stiffness matrices that are assumed to be diagonal matrices as shown below (j=s,r,c):

$$\mathbf{C}_b=\mathrm{Diag}\begin{bmatrix}\mathbf{c}_{bc} & \mathbf{c}_{br} & \mathbf{c}_{bs} & 0 & \dots & 0\end{bmatrix}, \tag{7a}$$

$$\mathbf{K}_b=\mathrm{Diag}\begin{bmatrix}\mathbf{k}_{bc} & \mathbf{k}_{br} & \mathbf{k}_{bs} & \mathbf{0} & \dots & \mathbf{0}\end{bmatrix}. \tag{7b}$$

Here, sub-matrices $\mathbf{c}_{bj}$=Diag[c_{xj} c_{yj} c_{uj}] and $\mathbf{k}_{bj}$=Diag[k_{xj} k_{yj} k_{uj}] are the diagonal damping and stiffness matrices of the bearing supporting central member j (j=s,r,c). If any central member j is allowed to float radially (i.e. not supported externally), then $k_{xj}\approx k_{yj}\approx 0$. If a central member is held stationary, then k_{uj} is assigned a large value representing the stiffness of the holding structure.

The forcing term at the right-hand side of Eq. (6a) consists of a mean force vector $\bar{\mathbf{F}}$ and an alternating (time-varying) force vector $\mathbf{F}(t)$, which are defined as

$$\bar{\mathbf{F}}=N\begin{bmatrix}\bar{\mathbf{f}}_c & \bar{\mathbf{f}}_r & \bar{\mathbf{f}}_s & 0 & \dots & 0\end{bmatrix}^T, \tag{8a}$$

$$\mathbf{F}(t)=\begin{Bmatrix} 0 \\ \sum_{i=1}^{N}\mathbf{f}_{rpi}^{(1)} \\ \sum_{i=1}^{N}\mathbf{f}_{spi}^{(1)} \\ \mathbf{f}_{sp1}^{(2)}-\mathbf{f}_{rp1}^{(2)} \\ \vdots \\ \mathbf{f}_{spN}^{(2)}-\mathbf{f}_{rpN}^{(2)} \end{Bmatrix}. \tag{8b}$$

Here $\mathbf{F}(t)$ contains all of the external displacement excitations $e_{spi}(t)$ and $e_{rpi}(t)$ at the gear mesh frequency as well as the excitations $E_{spi}(t)$, $E_{pis}(t)$, $E_{rpi}(t)$ and $E_{pir}(t)$ at the relative gear rotational frequencies.

2.2. Formulation of modulations of the excitations due to manufacturing errors

The error functions $E_{spi}(t)$, $E_{pis}(t)$, $E_{rpi}(t)$ and $E_{pir}(t)$ given in Eq. (1b) as part of the relative gear mesh displacements represent errors associated with rotational frequencies of gears relative to the carrier. Such errors include gear eccentricities, pitch-line run-out errors, tooth spacing and indexing errors, which are approximated here to harmonic forms for both the s–pi and r–pi meshes as

$$E_{spi}(t)=E_s\sin\left[\frac{\omega_m}{Z_s}t+\varepsilon_s-\psi_{si}\right], \tag{9a}$$

$$E_{pis}(t)=E_{pi}\sin\left[\frac{\omega_m}{Z_p}t+\varepsilon_{pi}-\alpha_s\right], \tag{9b}$$

$$E_{rpi}(t)=E_r\sin\left[\frac{\omega_m}{Z_r}t+\varepsilon_r+\psi_{ri}\right], \tag{9c}$$

$$E_{pir}(t)=E_{pi}\sin\left[\frac{\omega_m}{Z_p}t+\varepsilon_{pi}+\alpha_r\right]. \tag{9d}$$

Here, the gear mesh frequency is defined as ω_m=$Z_s|\omega_s-\omega_c|$=$Z_r|\omega_r-\omega_c|$=$Z_p|\omega_p-\omega_c|$, where ω_j and Z_j (j=r,s,p) are absolute nominal angular velocity and number of teeth of gear j and ω_c is the absolute nominal angular velocity of the carrier. Accordingly, the excitations $E_{pis}(t)$ and $E_{pir}(t)$ of pinion pi are at a frequency ω_m/Z_p that is equal to the rotational velocity of pi relative to c. Similarly, $E_{spi}(t)$ and $E_{rpi}(t)$ are at frequencies ω_m/Z_s and ω_m/Z_r, respectively, representing the rotational velocities of the sun and ring gears relative to the carrier. Coefficients E_s, E_r and E_{pi} are the amplitudes of these errors. The additional phase angles ε_s, ε_r and ε_{pi} illustrated in Fig. 1 define the initial orientation of them, as previously discussed.

In the absence of errors defined in Eqs. (9a)–(9d), gear transmission error excitations defined as a part of the gear mesh interfaces shown in Fig. 2(a) and (b) are given in periodic form as [27]

$$e_{spi}(t) = \sum_{\ell=1}^{L} e_{sp}^{(\ell)} \sin[\ell\omega_m t + \ell Z_s \psi_i + \phi_{sp}^{(\ell)}], \tag{10a}$$

$$e_{rpi}(t) = \sum_{\ell=1}^{L} e_{rp}^{(\ell)} \sin[\ell\omega_m t + \ell Z_r \psi_i + \ell\gamma_{sr} + \phi_{rp}^{(\ell)}] \tag{10b}$$

where γ_{sr} is the phase angle between $e_{spi}(t)$ and $e_{rpi}(t)$.

If the dynamic model proposed in the previous section were to be exercised with excitations as defined in Eqs. (9a)–(10b) as it was done in Ref. [27], one would observe little or no modulation sidebands in dynamic gear mesh forces $F_{spi}(t)$ and $F_{rpi}(t)$ as there is no apparent interaction between the two groups of excitations. In reality, however, the presence of errors defined by Eqs. (9a)–(9d) causes $e_{spi}(t)$ and $e_{rpi}(t)$ to be amplitude and frequency modulated, forming the basis for sidebands due to manufacturing errors of gears. In presence of errors defined in Eqs. (9a)–(9d), a quasi-static deformable body contact analysis of a typical automotive external gear pair using a gear load distribution model [28] shows that the peak-to-peak amplitude of $e_{spi}(t)$ might experience up to 4–6% variation due to $E_{spi}(t)$ and $E_{pis}(t)$ even with modest error magnitudes of E_s or E_{pi} (say 20 μm or less) depending on the instantaneous direction of the error of one gear with respect to the mating gear. In addition to this amplitude modulation, a frequency modulation is also resulted since the variation in effective center distance caused by these errors modulates the tooth meshing period. These indicate that Eqs. (10a) and(10b) must be modified in the presence of the gear errors defined in Eqs. (9a)–(9d).

In order to show the impact of $E_{spi}(t)$, $E_{pis}(t)$, $E_{rpi}(t)$ and $E_{pir}(t)$ on $e_{spi}(t)$ and $e_{rpi}(t)$, we consider only the fundamental harmonic of $e_{spi}(t)$ and $e_{rpi}(t)$ (i.e. L=1 in Eqs. (10a) and (10b) with $e_{sp}{}^{(1)}=e_{sp}$, $\phi_{sp}{}^{(1)}=\phi_{sp}$, $e_{rp}{}^{(1)}=e_{rp}$ and $\phi_{rp}{}^{(1)}=\phi_{rp}$). However, the below formulation can easily be expanded to include the higher harmonics as well. The excitations $e_{spi}(t)$ and $e_{rpi}(t)$ with amplitude and frequency modulations are written as

$$e_{spi}(t) = A_{spi}(t) e_{sp} \sin[B_{spi}(t)\omega_m t + Z_s \psi_i + \phi_{sp}], \tag{11a}$$

$$A_{spi}(t) = 1 + \beta_s \sin\left(\frac{\omega_m}{Z_s} t + \phi_{\beta si}\right) + \beta_{pi} \sin\left(\frac{\omega_m}{Z_p} t + \phi_{\beta pi}\right), \tag{11b}$$

$$B_{spi}(t) = 1 + \hat{\beta}_s \sin\left[\frac{\omega_m}{Z_s} t + \hat{\phi}_{\hat{\beta} si}\right] + \hat{\beta}_{pi} \sin\left[\frac{\omega_m}{Z_p} t + \hat{\phi}_{\hat{\beta} pi}\right] \tag{11c}$$

and

$$e_{rpi}(t) = A_{rpi}(t) e_{rp} \sin[B_{rpi}(t)\omega_m t + Z_r \psi_i + \gamma_{sr} + \phi_{rp}], \tag{12a}$$

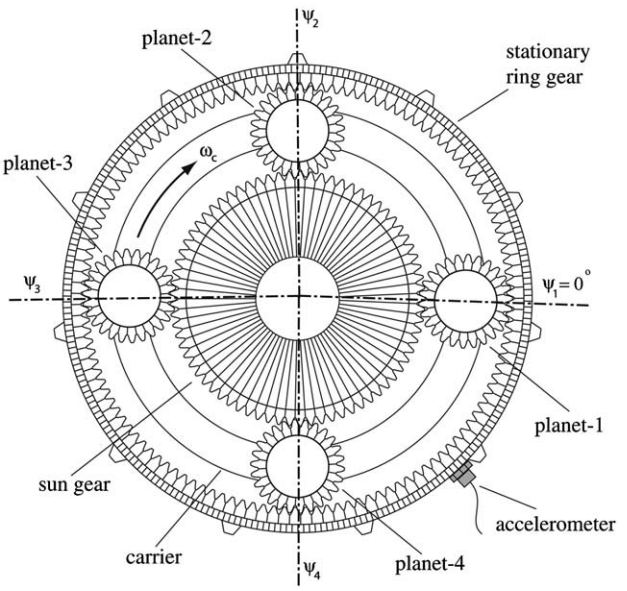

Fig. 3. Schematic illustration of a planetary gear set with four planets and an accelerometer mounted on the stationary ring gear.

$$A_{rpi}(t) = 1 + \beta_r \sin\left[\frac{\omega_m}{Z_r}t + \phi_{\beta ri}\right] + \vartheta_{pi} \sin\left[\frac{\omega_m}{Z_p}t + \phi_{\vartheta pi} + \pi\right], \tag{12b}$$

$$B_{rpi}(t) = 1 + \hat{\beta}_r \sin\left[\frac{\omega_m}{Z_r}t + \hat{\phi}_{\hat{\beta}r}\right] + \hat{\vartheta}_{pi} \sin\left[\frac{\omega_m}{Z_p}t + \hat{\phi}_{\hat{\vartheta}pi} + \pi\right]. \tag{12c}$$

Table 1
Basic design parameters of the example gear train.

Parameter	Sun	Planet	Ring
Number of teeth	80	30	140
Module (mm)	1.8	1.8	1.8
Pressure angle (deg)	22.5	22.5	22.5
Face width (mm)	30	30	30
Root diameter (mm)	131	43.4	237.2
Outside diameter (mm)	139.2	50	229.6
Pin circle diameter (mm)	78		
Tooth thickness (mm)	2.83	2.85	2.97
Operating center dis. (mm)	92.1	92.1	

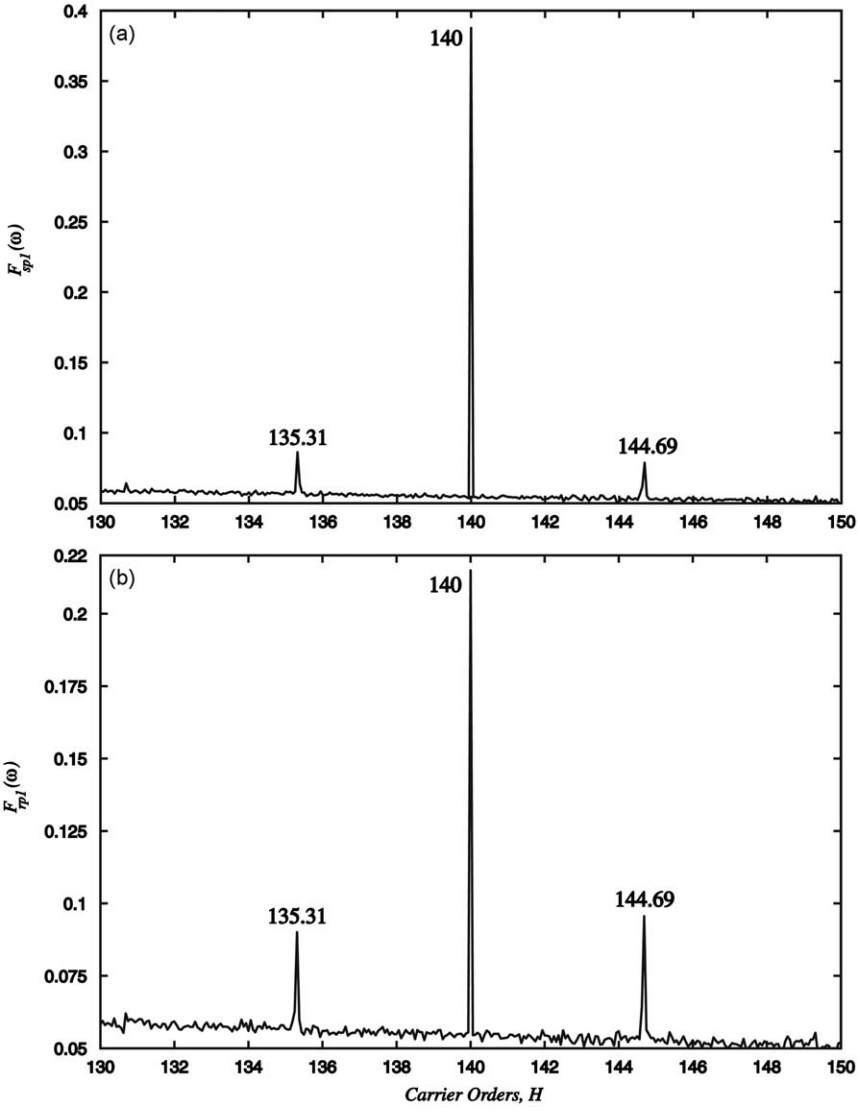

Fig. 4. Predicted (a) $F_{sp1}(\omega)$ and (b) $F_{rp1}(\omega)$ spectra for the example planetary gear set under the influence of AM due to planet-1 run-out error with β_{p1}=0.034, $\phi_{\beta p1}$=3π/2, ϑ_{p1}=0.033, $\phi_{\vartheta p1}$=π/2, κ_{p1}=0.055, $\phi_{\kappa p1}$=3π/2, τ_{p1}=0.049 and $\phi_{\tau p1}$=π/2.

Here, dimensionless coefficients β_s and β_{pi} represent the amplitude modulation of the fundamental harmonic of $e_{spi}(t)$ due to the errors of the sun gear and planet *pi*, and $\phi_{\beta si}$ and $\phi_{\beta pi}$ are the phase angles for the same gears, as defined by the initial position angles ε_s and ε_{pi}. Parameters β_r and $\phi_{\beta ri}$ define the amplitude and the phase angle of the amplitude modulation of $e_{rpi}(t)$ due to the error of the ring gear. Parameters ϑ_{pi} and $\phi_{\vartheta pi}$ define the amplitude and the phase angle of the amplitude modulation of $e_{rpi}(t)$ due to the error of the planet gear. Here, it is important to note that the amplitude modulation coefficients (β_{pi} and ϑ_{pi}) are usually different for the *s–pi* and *r–pi* meshes involving the same planet *pi* for the same planet run-out amount. Similarly, amplitude coefficients, $\hat{\beta}_s$, $\hat{\beta}_r$, $\hat{\beta}_{pi}$ and $\hat{\vartheta}_{pi}$ and the phase angles $\hat{\phi}_{\hat{\beta}si}$, $\hat{\phi}_{\hat{\beta}ri}$, $\hat{\phi}_{\hat{\beta}pi}$ and $\hat{\phi}_{\hat{\vartheta}pi}$ define the frequency modulations of $e_{spi}(t)$ and $e_{rpi}(t)$.

All these modulation parameters can be defined up-front by simulating the loaded gear contacts under quasi-static conditions [28]. In Eqs. (11a)–(12c), the gear mesh-frequency excitations $e_{spi}(t)$ and $e_{rpi}(t)$ are both amplitude and frequency modulated by errors at rotational frequencies of gear *s*, *r* and *pi* relative to the planet carrier. These rotational frequencies ω_m/Z_s, ω_m/Z_r and ω_m/Z_p are typically distinct so that sidebands caused by each on the resultant $F_{spi}(t)$ and $F_{rpi}(t)$ spectra should correspond to a different set of frequencies, as it will be demonstrated later.

The same modulation mechanism affects the periodically varying gear mesh stiffness functions of the *s–pi* and *r–pi* meshes in the same way. In their unmodulated form, these functions are defined below as

$$k_{spi}(t) = \bar{k}_{sp}\{1 + \sum_{\ell=1}^{L} k_{sp}^{(\ell)} \sin[\ell\omega_m t + \ell Z_s \psi_i + \ell\Gamma + \phi_{sp}^{(\ell)}]\}, \tag{13a}$$

$$k_{rpi}(t) = \bar{k}_{rp}\{1 + \sum_{\ell=1}^{L} k_{rp}^{(\ell)} \sin[\ell\omega_m t + \ell Z_r \psi_i + \ell\Gamma + \ell\gamma_{sr} + \phi_{rp}^{(\ell)}]\}. \tag{13b}$$

Here, $\bar{k}_{sp}$ and $\bar{k}_{rp}$ are the mean mesh stiffness values computed at a given torque value, $k_{sp}{}^{(\ell)}$ and $k_{rp}{}^{(\ell)}$ are the dimensionless ℓth harmonic amplitudes, and Γ is the phase angle between $e_{spi}(t)$ and $k_{spi}(t)$ (and also between $e_{rpi}(t)$ and $k_{rpi}(t)$). Considering only the fundamental harmonic terms (L=1) for demonstration purposes and modulating the amplitudes and the mesh frequency the same way as in Eqs. (11a)–(12c), one obtains

$$k_{spi}(t) = \bar{k}_{sp} + C_{spi}(t) k_{sp} \sin[D_{spi}(t)\omega_m t + Z_s \psi_i + \Gamma + \phi_{sp}], \tag{14a}$$

$$C_{spi}(t) = 1 + \kappa_s \sin\left[\frac{\omega_m}{Z_s} t + \phi_{\kappa si}\right] + \kappa_{pi} \sin\left[\frac{\omega_m}{Z_p} t + \phi_{\kappa pi}\right], \tag{14b}$$

$$D_{spi}(t) = 1 + \hat{\kappa}_s \sin\left[\frac{\omega_m}{Z_s} t + \hat{\phi}_{\hat{\kappa} si}\right] + \hat{\kappa}_{pi} \sin\left[\frac{\omega_m}{Z_p} t + \hat{\phi}_{\hat{\kappa} pi}\right] \tag{14c}$$

and

$$k_{rpi}(t) = \bar{k}_{rp} + C_{rpi}(t) k_{rp} \sin[D_{rpi}(t)\omega_m t + Z_r \psi_i + \gamma_{sr} + \Gamma + \phi_{rp}], \tag{15a}$$

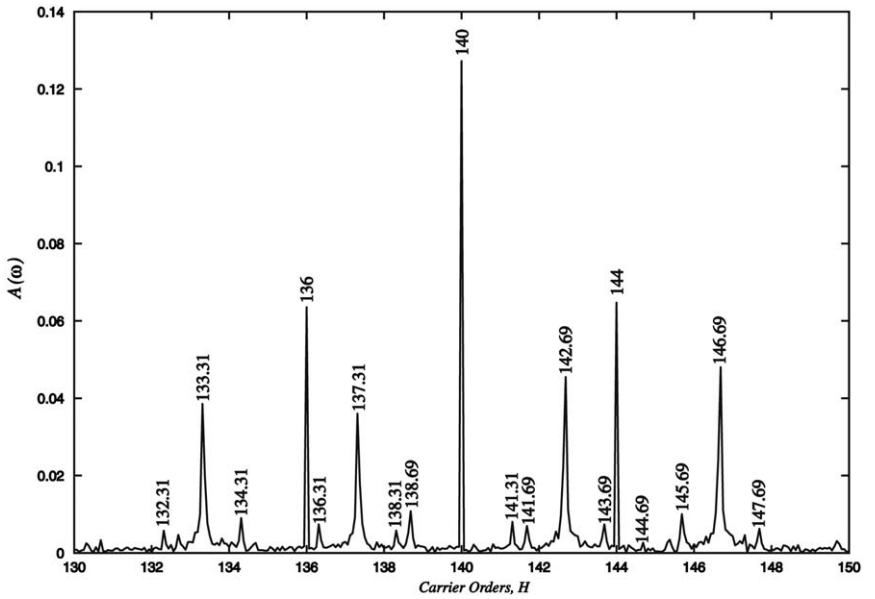

Fig. 5. Predicted $A(\omega)$ spectra for the example planetary gear set with a rotating carrier under the influence of AM due to planet-1 run-out error with β_{p1}=0.034, $\phi_{\beta p1}$=3π/2, ϑ_{p1}=0.033, $\phi_{\vartheta p1}$=π/2, κ_{p1}=0.055, $\phi_{\kappa p1}$=3π/2, τ_{p1}=0.049 and $\phi_{\tau p1}$=π/2.

$$C_{rpi}(t) = 1 + \kappa_r \sin\left[\frac{\omega_m}{Z_r}t + \phi_{\kappa ri}\right] + \tau_{pi} \sin\left[\frac{\omega_m}{Z_p}t + \phi_{\tau pi} + \pi\right], \tag{15b}$$

$$D_{rpi}(t) = 1 + \hat{\kappa}_r \sin\left[\frac{\omega_m}{Z_r}t + \hat{\phi}_{\hat{\kappa} ri}\right] + \hat{\tau}_{pi} \sin\left[\frac{\omega_m}{Z_p}t + \hat{\phi}_{\hat{\tau} pi} + \pi\right]. \tag{15c}$$

2.3. Formulation of modulations due to rotating carrier

With the modulated excitations defined by Eqs. (11a)–(15c), the equations of motion (6a) of the nonlinear time-varying planetary gear system are solved by using direct numerical integration technique to determine the unknown vector of displacement time histories $\mathbf{Q}(t)$, from which the dynamic gear mesh forces $F_{spi}(t)$ and $F_{rpi}(t)$ can be computed according to Eq. (1a). As it will be demonstrated in the next section, these gear mesh forces exhibit sideband activity associated with the once-per-revolution errors of the gears. If the power flow configuration is such that the carrier is held stationary (i.e. sun and ring gears serve as input and output members), then any vibration or noise spectra measured in a fixed location in the vicinity of the gear set will have the same sideband structure. As described in Ref. [4], another layer of modulations take place when the carrier is rotating, as the influence of gear mesh forces (now rotating with the carrier) are amplitude

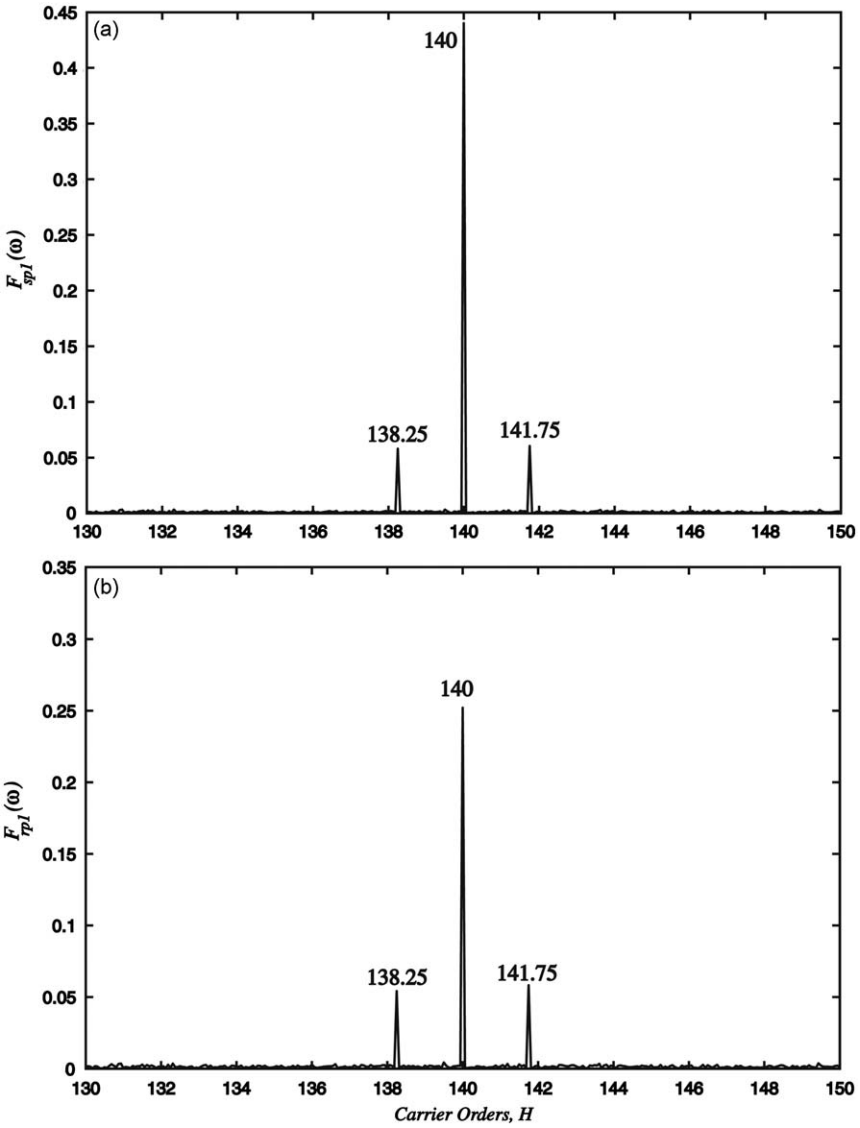

Fig. 6. Predicted (a) $F_{sp1}(\omega)$ and (b) $F_{rp1}(\omega)$ spectra for the example planetary gear set under the influence of AM due to sun gear run-out error with β_{si}=0.0338 ($i \in [1,4]$), $\phi_{\beta s1}=\pi/2$, $\phi_{\beta s2}=0$, $\phi_{\beta s3}=3\pi/2$, $\phi_{\beta s4}=\pi$ and κ_{si}=0.0547 ($i \in [1,4]$), $\phi_{\kappa s1}=\pi/2$, $\phi_{\kappa s2}=0$, $\phi_{\kappa s3}=3\pi/2$ and $\phi_{\kappa s4}=\pi$.

modulated viewed from a fixed measurement point. The predicted $F_{spi}(t)$ and $F_{rpi}(t)$ with or without the other gear errors can be used as input in this earlier formulation [4] to predict the resultant spectra at a fixed point for the rotating carrier case. Referring to Ref. [4] for the details, a brief summary of this formulation will be provided here for completeness purposes.

Consider the same planetary gear set with N planets positioned at angles ψ_i ($i \in [1,N]$) and with rotating carrier c and the sun gear s (fixed: ring gear r). For a complete revolution of the carrier, a transducer positioned on the housing shown in Fig. 3 experiences the disturbances from all $2N$ planet meshes in sequence. As the force transmission path between the meshes of planet pi and the fixed transducer location varies in time as the carrier rotates, the influence of each planet on the transducer was limited in Ref. [4] to a duration of T_c/N, where $T_c=2\pi/\omega_c$ is the rotational period of the carrier. This gradually increasing and then decaying dominance of the forces of planet pi within a T_c/N time period, was approximated by weighting function in the form of a Hanning window $w(t)=0.5-0.5\cos(2\pi Nt/T_c)$ as

$$w_i(t) = w\left(t - \frac{\psi_i}{2\pi}T_c\right)\sum_{n=1}^{\infty}\left\{u\left[t - \left(\frac{(n-1)N+i-1}{N}\right)T_c\right] - u\left[t - \left(\frac{(n-1)N+i}{N}\right)T_c\right]\right\}, \tag{16}$$

where ψ_i is the position angle of planet pi. In this equation, terms $u(t-a)$ are unit step functions $u(t-a)=1$ for $t>a$ and $u(t-a)=0$ for $t<a$) that ensure the influence of planet pi on the transducer lasts only for a period of T_c/N. The summation over n ensures the periodicity of the function.

The acceleration signal at the transducer location caused by dynamic forces $F_{spi}(t)$ and $F_{rpi}(t)$ of the meshes of planet pi mesh are then defined as

$$a_i(t) = S_s w_i(t) F_{spi}(t) + S_r w_i(t) F_{rpi}(t), \tag{17}$$

where S_s are S_r constants facilitated to establish the relation between the gear mesh forces and the resultant acceleration at a given rotational position. The total acceleration signal $a(t)$ is given as

$$a(t) = \sum_{i=1}^{N} a_i(t) \tag{18a}$$

with the corresponding frequency spectrum

$$A(\omega) = \left|\int_{-\infty}^{\infty} a(t)e^{-i\omega t}\,dt\right|. \tag{18b}$$

For the case of non-rotating carrier, all $w_i(t)=1$ with different S_s are S_r values for each planet depending on their distance from the transducer location.

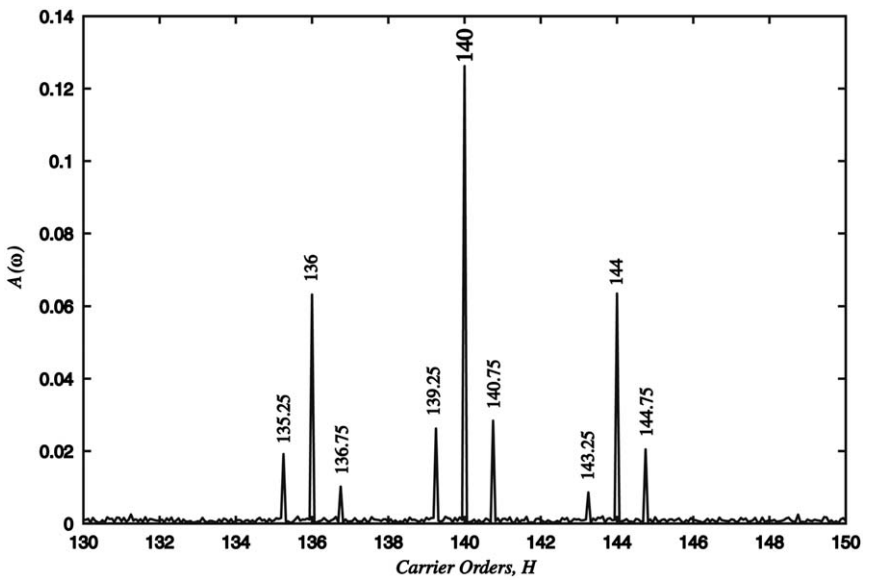

Fig. 7. Predicted $A(\omega)$ spectra for the example planetary gear set with a rotating carrier under the influence of AM due to sun gear run-out error with $\beta_{si}=0.0338$ ($i \in [1,4]$), $\phi_{\beta s1}=\pi/2$, $\phi_{\beta s2}=0$, $\phi_{\beta s3}=3\pi/2$, $\phi_{\beta s4}=\pi$ and $\kappa_{si}=0.0547$ ($i \in [1,4]$), $\phi_{\kappa s1}=\pi/2$, $\phi_{\kappa s2}=0$, $\phi_{\kappa s3}=3\pi/2$ and $\phi_{\kappa s4}=\pi$.

3. Example analysis of modulation sidebands of a planetary gear set with errors

In this section, an example planetary gear set is used to demonstrate different modulation mechanisms for systems with and without a rotating carrier under different dynamic conditions. The first step in this simulation is to determine the gear and carrier inertias and masses as well as bearing stiffnesses. The gear mesh interface parameters including the excitation terms defined in Eqs. (11a)–(15c) are then predicted under quasi-static conditions using a gear load distribution model similar to the one proposed in Ref. [28]. With these parameters and operating speed and load conditions in place, the system equations defined by Eqs. (6a)–(6e) are constructed and solved by using direct numerical integration to find the dynamic gear mesh forces defined in Eq. (1a). Finally, these forces are implemented in Section 2.3 to induce the amplitude modulations due to the rotation of the planet carrier.

Here, a 4-planet planetary gear set is chosen as the example system having gears with tooth counts Z_r=140, Z_s=80 and Z_p=30. Gear mesh parameters of $\bar{k}_{sp}$=5.2(10)^8 N/m, $k_{sp}^{(1)}$=17.5(10)^6 N/m, $\bar{k}_{rp}$=5.5(10)^8 N/m, $k_{rp}^{(1)}$=18.6(10)^6 N/m, $e_{sp}^{(1)}$=0.5 μm and $e_{rp}^{(1)}$=0.16 μm are used for harmonic forms of the mesh stiffness and transmission error excitations. Other parameters of this gear set that are relevant to the dynamic model are listed in Table 1. Here, the planets are equally spaced (ψ_i=2π(i−1)/4) and planet meshes are in-phase type (Z_s/N=integer and Z_r/N=integer) such that this gear set falls into the case (i) category according to the classification of planetary gear sets based on their sideband behavior proposed in Ref. [4]. Planetary gear sets in this category were shown to have a relatively simple sideband activity due to the carrier rotation. This

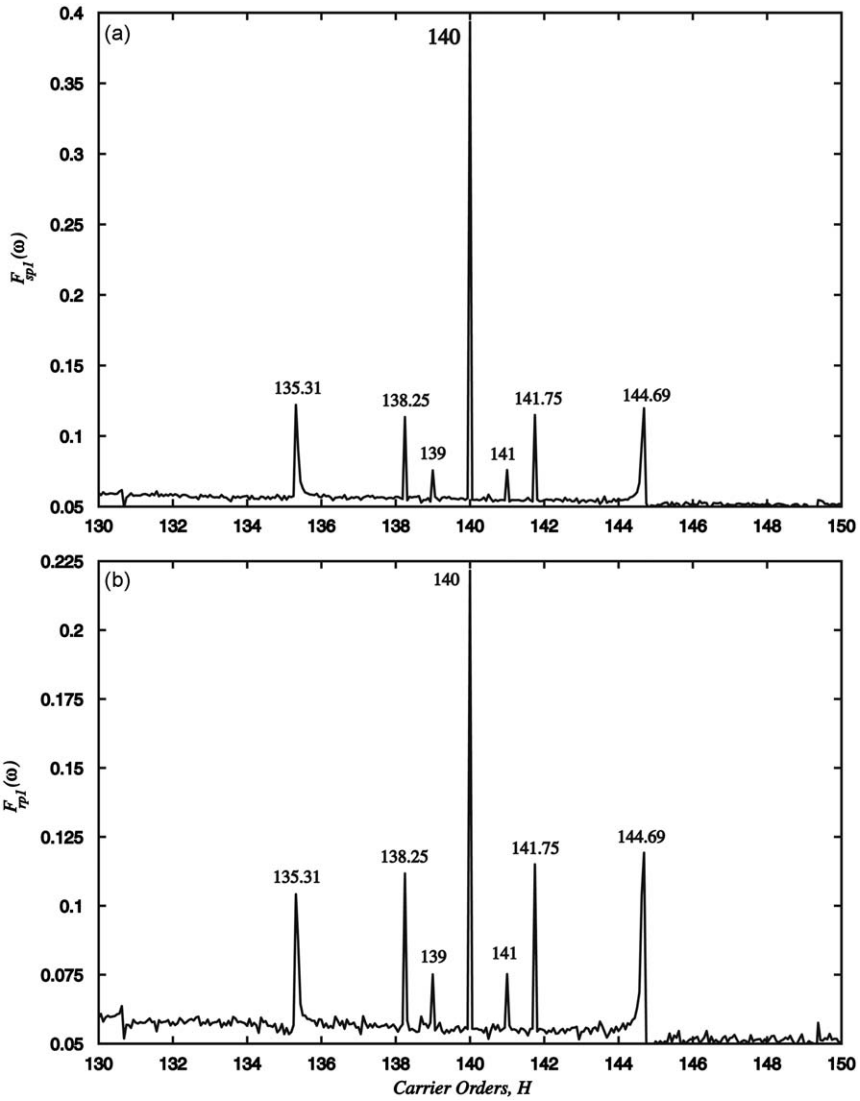

Fig. 8. Predicted (a) $F_{sp1}(\omega)$ and (b) $F_{rp1}(\omega)$ spectra for the example planetary gear set under the influence of AM due to planet-1, sun and ring gear run-out errors. β_{ri}=0.0332 ($i\in$[1,4]), $\phi_{\beta r1}$=3π/2, $\phi_{\beta r2}$=0, $\phi_{\beta r3}$=π/2, $\phi_{\beta r4}$=π, κ_{ri}=0.0491 (i=1,…,4), $\phi_{\kappa r1}$=3π/2, $\phi_{\kappa r2}$=0, $\phi_{\kappa r3}$=π/2, and $\phi_{\kappa r4}$=π, and sun and planet related parameters are as in Figs. 4 and 6.

will allow a more clear demonstration of the sidebands due to manufacturing errors with limited added complexity due to carrier rotations, while the model is capable of handling any of five categories proposed in Ref. [4]. For the same reason, AM and FM modulations will be introduced separately with one gear error at a time. Both dynamic gear mesh force spectra and the vibration spectra at a fixed point will be predicted to identify the impact of the rotating carrier. Finally, simulations will be performed at different speeds (frequencies) representing off-resonance and near resonance conditions to highlight the impact of dynamic behavior on the planetary sideband activity.

3.1. Planetary gear set modulations under off-resonance conditions

The undamped natural modes of the corresponding linear time-invariant system can be determined by setting $\mathbf{C}=\mathbf{0}$ and $\mathbf{C}_b=\mathbf{0}$ in Eq. (6a), considering constant gear mesh stiffnesses with $k_{spi}(t)=\bar{k}_{sp}$ and $k_{rpi}(t)=\bar{k}_{rp}$ in Eqs. (14a) and (15a), and solving the corresponding eigenvalue problem. With the numerical values of the parameters defined above and in Table 1, first five natural frequencies of this example gear set are determined as 982, 2484, 2629, 5088 and 5101 Hz, excluding the rigid-body mode at 0 Hz. Here, some of these modes are repeated planet modes where planets displace in sequentially-phased manner while central members are motionless. The rest are in-phase, overall modes where each planet has the same motion relative to central members [5,6]. First, the example planetary gear set is simulated at a lower mesh frequency of 400 Hz (ω_s=49.5 rad/s) resulting in ω_m=2513 rad/s in this kinematic configuration with a stationary ring gear such that a typical off-resonance condition exists. Under these conditions, the gear set acts as a linear time-varying system with no tooth separations and nonlinear behavior. All of the analyses are carried out at a sun torque value of T_s=500 N m. This corresponds to about 42% of the rated maximum torque of this planetary gear set in an actual automatic transmission.

First, a planet run-out error of E_{p1}=20 μm at ε_{p1}=0 is applied to planet $p1$ while the other E_{pi}=0 and E_s=E_r=0. The corresponding amplitude modulation parameters in Eqs. (11a)–(12c), (14a)–(15c) are defined using the gear load distribution model [28] as β_{p1}=0.034, $\phi_{\beta p1}$=3π/2, ϑ_{p1}=0.033, $\phi_{\vartheta p1}$=π/2, κ_{p1}=0.055, $\phi_{\kappa p1}$=3π/2, τ_{p1}=0.049 and $\phi_{\tau p1}$=π/2 with all other modulation coefficients are set to zero. Predicted dynamic mesh force spectra $F_{sp1}(\omega)$ and $F_{rp1}(\omega)$ at s–$p1$ and r–$p1$ meshes are shown in Fig. 4. In these figures, the x-axis represents the output side gear mesh orders obtained by normalizing the frequency scale by the rotational output (carrier) frequency. With this, the fundamental gear mesh order is H_m=Z_r=140. Two almost symmetric sidebands are evident at both sides of H_m at orders of $H_m \pm H_{p/c}$ where $H_{p/c}$=Z_r/Z_p=4.69. Dynamic mesh force spectra for the meshes of planets $p2$ to $p4$ are also very similar to those shown in Fig. 4 for the meshes of the first planet.

With these gear mesh forces, $F_{spi}(t)$ and $F_{rpi}(t)$ ($i\in[1,N]$), predicted with the sidebands associated with E_{p1}, the procedure outlined in Section 2.3 is applied next to predict the acceleration spectra that would be measured on the stationary ring gear as illustrated in Fig. 3. Fig. 5 shows the predicted acceleration spectrum $A(\omega)$ for this case, given S_s=0 and S_r=1 in Eq. (17). Here, some of the energy of the gear mesh harmonic order of H=H_m=140 is distributed to two sidebands at H=$H_m \pm N$=140 ± 4 as a direct result of the amplitude modulation caused by the rotating carrier [4]. As the run-out (or eccentricity) vector rotates with the planet gear, it has a different phase angle each time the planet enters its windowed

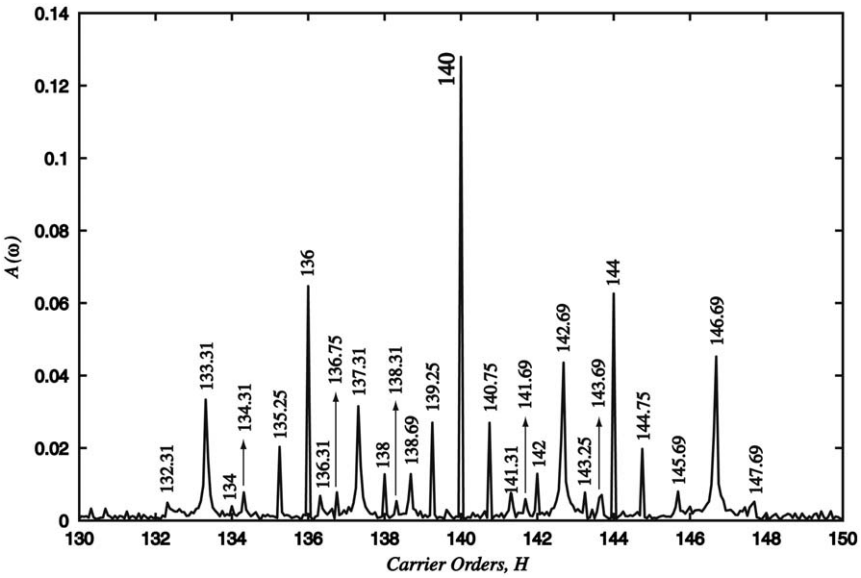

Fig. 9. Predicted $A(\omega)$ spectra for the example planetary gear set with a rotating carrier under the influence of AM due to planet-1, sun and ring gear run-out errors β_{ri}=0.0332 ($i\in[1,4]$), $\phi_{\beta r1}$=3π/2, $\phi_{\beta r2}$=0, $\phi_{\beta r3}$=π/2, $\phi_{\beta r4}$=π, κ_{ri}=0.0491 (i=1,…,4), $\phi_{\kappa r1}$=3π/2, $\phi_{\kappa r2}$=0, $\phi_{\kappa r3}$=π/2, and $\phi_{\kappa r4}$=π, and sun and planet related parameters are as in Figs. 4 and 6.

region. This causes the force sidebands at orders $H_m \pm H_{p/c}$ of Fig. 4 (135.31 and 144.69) to cause new sidebands at $H_m \pm H_{p/c} \pm n$ (n=integer) while orders $H_m \pm H_{p/c}$ disappear. Among them, the sideband orders $H_m \pm H_{p/c} \pm 2$ (H=133.31, 137.31, 142.69 and 146.69) are especially large in addition to those at $H_m \pm H_{p/c} \pm 2 \pm N$ (e.g. H=129.31, 141.31, 138.69 and 150.69).

Next, error amplitude of E_s=20 μm is applied to the sun gear of the same gear set while all E_{pi}=0 and E_r=0 at T_s=500 N m. Considering only the amplitude modulations in Eqs. (11a)–(11c), (14a) and (14b), the dynamic mesh forces are amplitude modulated due to the modulation parameters β_{si}=0.0338 ($i \in [1,4]$) with $\phi_{\beta s1}=\pi/2$, $\phi_{\beta s2}=0$, $\phi_{\beta s3}=3\pi/2$, $\phi_{\beta s4}=\pi$ and κ_{si}=0.0547 ($i \in [1,4]$) with $\phi_{\kappa s1}=\pi/2$, $\phi_{\kappa s2}=0$, $\phi_{\kappa s3}=3\pi/2$, $\phi_{\kappa s4}=\pi$. Predicted $F_{sp1}(\omega)$ and $F_{rp1}(\omega)$ for this case are shown in Fig. 6. Sideband orders at H=138.25 and 141.75 are evident in these force spectra. They correspond to orders $H=H_m \pm H_{s/c}$ where $H_{s/c}=Z_r/Z_s$=1.75. The corresponding acceleration spectrum $A(\omega)$ is shown in Fig. 7. Here, besides the orders at $H=H_m \pm N$=136 and 144, which are due to rotation of the carrier, some additional sidebands appear at $H=H_m \pm H_{p/c} \pm n$ due to the amplitude modulation of the sidebands shown in Fig. 6. Orders at H=139.25 and 140.75 are of this kind. It is also noted here that, among these orders, $H=H_m \pm H_{s/c} \pm 1 \pm N$ (e.g. orders 135.25, 136.75, 143.25 and 144.75) have reasonably large amplitudes.

Likewise, a non-zero E_r on the ring gear causes $F_{sp1}(\omega)$ and $F_{rp1}(\omega)$ sidebands at orders $H_m \pm H_{r/c}$ where $H_{r/c}$=1 as ring gear is fixed in this configuration. The corresponding $A(\omega)$ spectrum contains some additional sidebands at $H=H_m \pm H_{r/c} \pm n$. Figures for the case of ring gear error are not included here since they are qualitatively similar to those for the sun and planet gear errors. Instead, predictions for a case when $E_{p1}=E_s=E_r$=20 mm (all other E_{pi}=0 and $\varepsilon_{pi}=\varepsilon_s=\varepsilon_r$=0) are included here with all of the corresponding modulation parameters specified above used simultaneously. The resultant mesh force

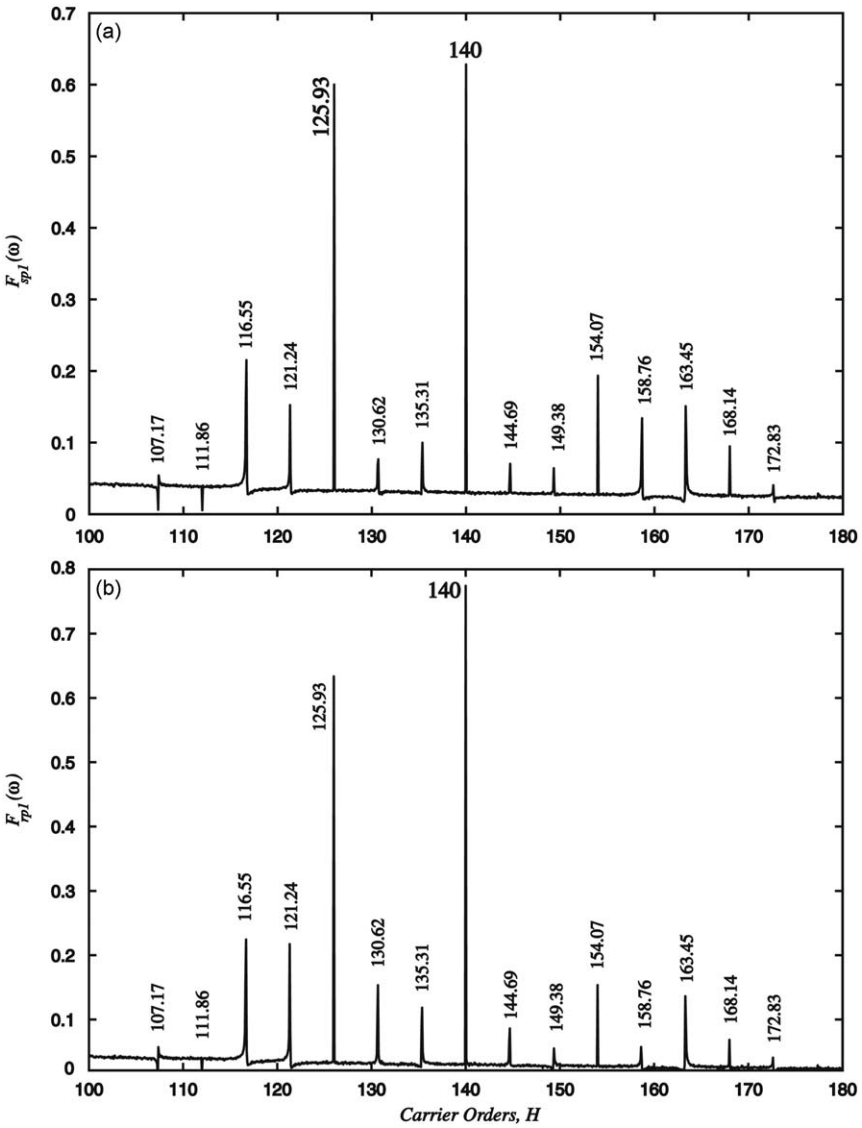

Fig. 10. Predicted (a) $F_{sp1}(\omega)$ and (b) $F_{rp1}(\omega)$ spectra for the example planetary gear set when only FM are present due to planet-1 run-out with $\hat{\beta}_{p1}=\hat{\vartheta}_{p1}=\hat{\kappa}_{p1}=\hat{\tau}_{p1}=8.5(10)^{-5}$, $\phi_{\hat{\beta}p1}=3\pi/2$, $\phi_{\hat{\vartheta}p1}=\pi/2$, $\phi_{\hat{\kappa}p1}=3\pi/2$ and $\phi_{\hat{\tau}p1}=\pi/2$.

spectra shown in Fig. 8 indicate that the sidebands created due to each individual error are linearly superimposed. The same statement is true for the corresponding $A(\omega)$ as well, as shown in Fig. 9. Here, all of the sideband groups identified above for each error, $H_m \pm H_{s/c} \pm n$, $H_m \pm H_{r/c} \pm n$ and $H_m \pm H_{p/c} \pm n$ (n: integer) coexist. It is also noted here that this $A(\omega)$ spectrum can be used to identify any sources of error in a planetary gear set as long as orders $H_{p/c}$, $H_{s/c}$ and $H_{r/c}$ are distinct. Only time these orders are not distinct is when Z_p=Z_s, resulting in $H_{p/c}$=$H_{s/c}$. In this special case, it would not be possible to separate the sideband orders caused by sun gear and planet gear errors.

Up to this point in this example analysis, only the amplitude modulations of the excitation functions due to manufacturing errors were considered. The same procedure will be used next to investigate the impact of the FM parameters in Eqs. (11a)–(12c), (14a)–(15c), with AM parameters intentionally turned off. For the first case of the planet gear run-out error of E_{p1}=20 μm with ε_{p1}=0, FM parameters are estimated as $\hat{\beta}_{p1} = \hat{\vartheta}_{p1} = \hat{\kappa}_{p1} = \hat{\tau}_{p1} = 8.5(10)^{-5}$, $\phi_{\hat{\beta}p1} = 3\pi/2$, $\phi_{\hat{\vartheta}p1} = \pi/2$, $\phi_{\hat{\kappa}p1} = 3\pi/2$, and $\phi_{\hat{\tau}p1} = \pi/2$. The resultant $F_{sp1}(\omega)$ and $F_{rp1}(\omega)$ are shown in Fig. 10 for T_s=500 N m. Instead of creating a single pair of sidebands as it was in the case of AM in Fig. 4, a large number of sidebands are created by the frequency modulation of the gear mesh excitations. The FM sidebands ultimately appear at orders $H_m \pm nH_{p/c}$. However, in cases where relatively large frequency modulation parameters are used, additional orders show up possibly at orders $H_m \pm nH_{p/c} \pm \hat{\beta}_{pi}H_m$. It is also observed from these two spectra that sidebands with significant amplitudes

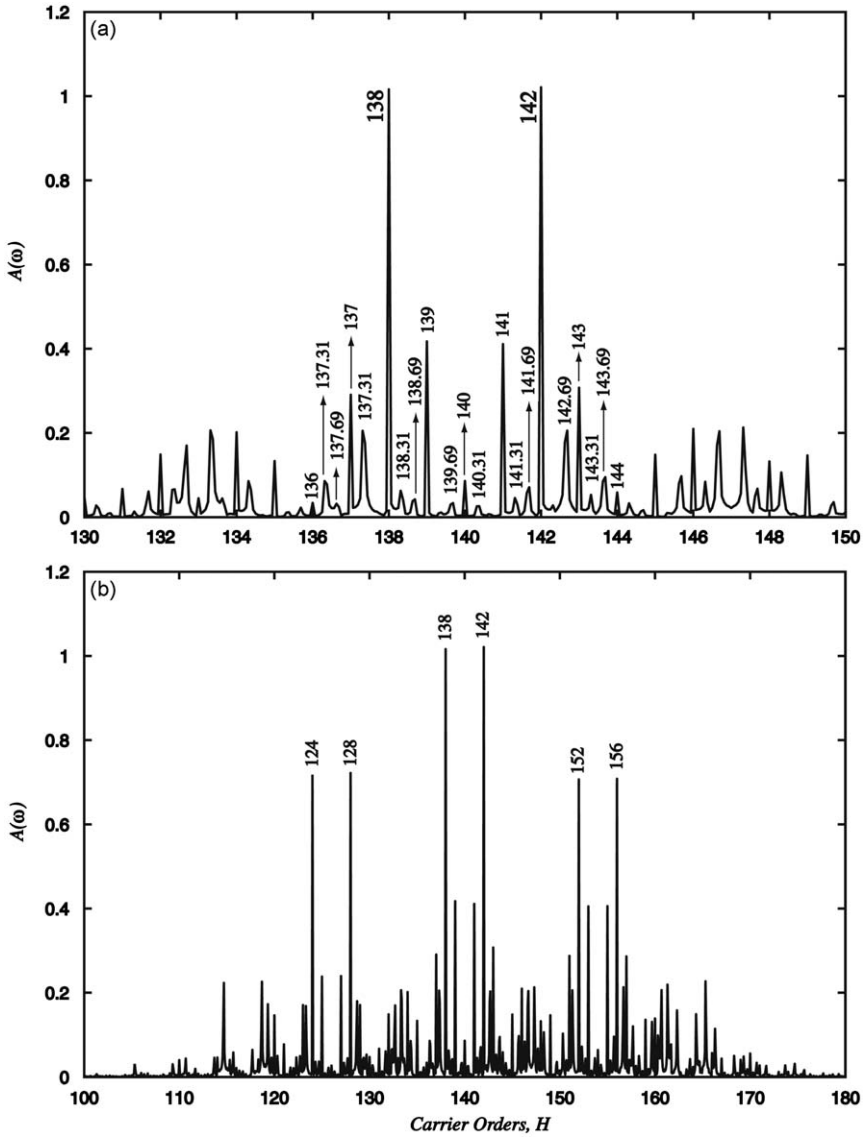

Fig. 11. Predicted $A(\omega)$ spectrum for the example planetary gear set when only FM are present due to planet-1 run-out with $\hat{\beta}_{p1} = \hat{\vartheta}_{p1} = \hat{\kappa}_{p1} = \hat{\tau}_{p1} = 8.5(10)^{-5}$, $\phi_{\hat{\beta}p1} = 3\pi/2$, $\phi_{\hat{\vartheta}p1} = \pi/2$, $\phi_{\hat{\kappa}p1} = 3\pi/2$ and $\phi_{\hat{\tau}p1} = \pi/2$: (a) a zoomed in view in the vicinity of the fundamental gear mesh frequency and (b) the same spectrum with a wider frequency range.

range from H=115–165. The corresponding $A(\omega)$ spectrum at a fixed transducer location is shown in Fig. 11. Here, fundamental mesh harmonic order at H_m=140 is split into orders 138 and 142. In Fig. 11(b) that displays the same spectrum in a wider frequency range, significant sideband orders at $H_m \pm nH_{p/c} \pm nN$ appear in addition to the ones at orders $H_m \pm nH_{p/c}$.

Secondly, a sun gear run-out error with E_s=20 μm starting at the initial position angle of ε_s=0° is introduced to the system operating at T_s=500 N m. Only the FM parameters ($\hat{\beta}_s = \hat{\kappa}_s = 3.0(10)^{-5}$, $i \in [1,4]$, $\phi_{\hat{\beta}s1} = \phi_{\hat{\kappa}s1} = \pi/2$, $\phi_{\hat{\beta}s2} = \phi_{\hat{\kappa}s2} = 0$, $\phi_{\hat{\beta}s3} = \phi_{\hat{\kappa}s3} = 3\pi/2$ and $\phi_{\hat{\beta}s4} = \phi_{\hat{\kappa}s4} = \pi$) are included here in order to demonstrate the sole influence of frequency modulations. The predicted $F_{sp1}(\omega)$ and $F_{rp1}(\omega)$ are shown in Fig. 12. The FM sidebands typically appear at orders $H_m \pm nH_{s/c}$. Meanwhile, Fig. 13 shows the corresponding $A(\omega)$ spectrum, exhibiting sidebands in a narrower order range of $H_m \pm 10$, which represents a much narrower frequency range than that of Fig. 11. This is simply because the value of the modulation parameter $\hat{\beta}_s$ in Figs. 12 and 13 is smaller than the value of $\hat{\beta}_{pi}$ corresponding to Figs. 10 and 11. Fig. 13(a) shows dominant sidebands at orders $H_m \pm nH_{s/c} \pm 2$ as well as $H_m \pm nH_{s/c} \pm 2 \pm n$ and $H_m \pm nH_{s/c} \pm 2 \pm N$, besides the ones at $H_m \pm N$.

Similar to the previous two cases, a non-zero E_r on the ring gear causes gear mesh force sideband orders at $H_m \pm nH_{r/c}$. The corresponding $A(\omega)$ spectrum contains some additional sidebands at $H = H_m \pm nH_{r/c} \pm n$. Again, figures for the case of ring gear error are not included here since they are qualitatively similar to those for the sun and planet gear errors. Instead, FM predictions for a case when E_{p1}=E_s=E_r=20 μm (all other E_{pi}=0 and ε_{pi}=ε_s=ε_r=0) are included here with all of the corresponding

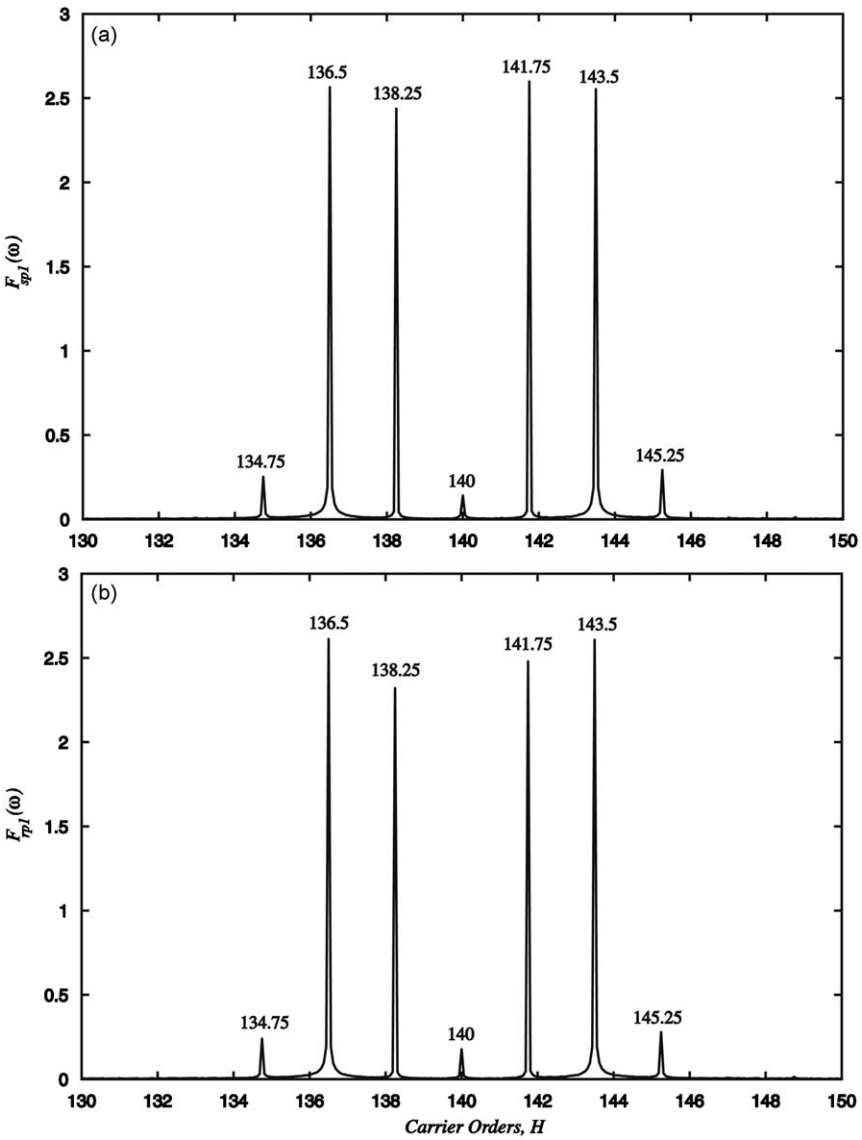

Fig. 12. Predicted (a) $F_{sp1}(\omega)$ and (b) $F_{rp1}(\omega)$ spectra for the example planetary gear set when only FM are present due to sun gear run-out with $\hat{\beta}_s = \hat{\kappa}_s = 3.0(10)^{-5}$, $i \in [1,4]$, $\phi_{\hat{\beta}s1} = \phi_{\hat{\kappa}s1} = \pi/2$, $\phi_{\hat{\beta}s2} = \phi_{\hat{\kappa}s2} = 0$, $\phi_{\hat{\beta}s3} = \phi_{\hat{\kappa}s3} = 3\pi/2$ and $\phi_{\hat{\beta}s4} = \phi_{\hat{\kappa}s4} = \pi$.

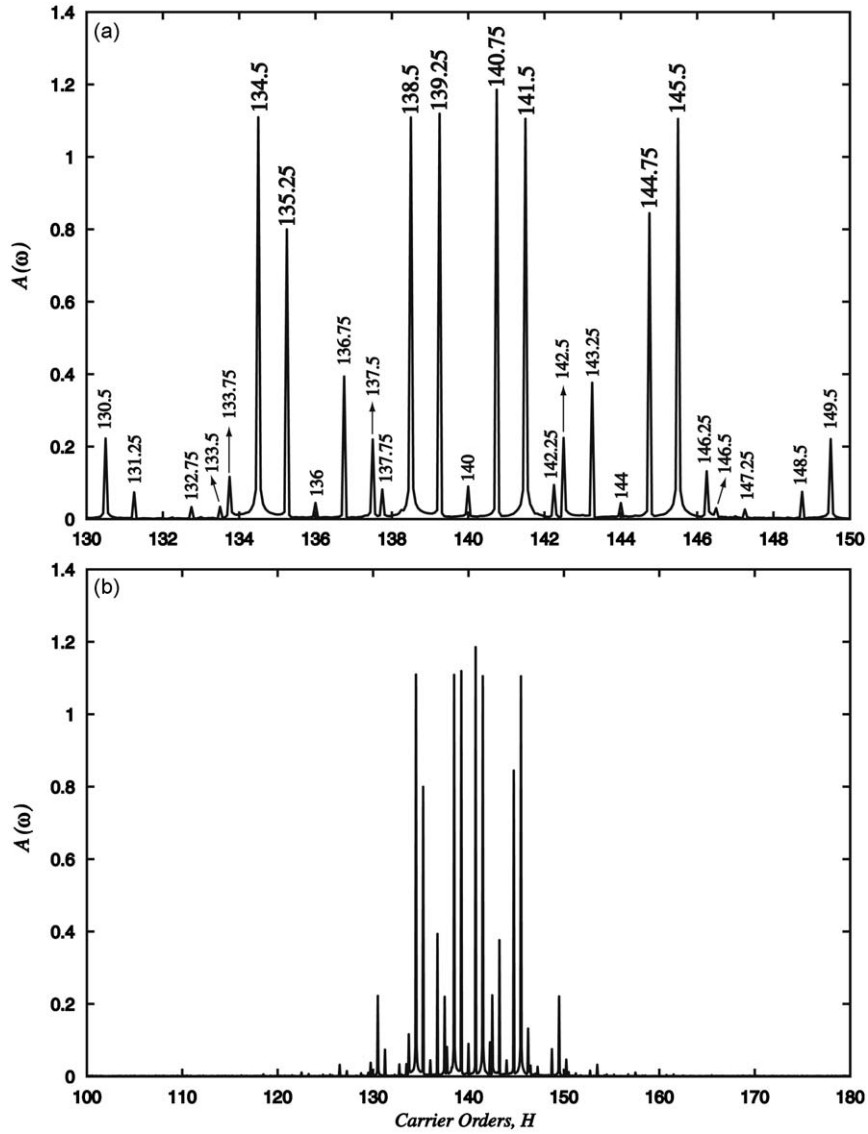

Fig. 13. Predicted $A(\omega)$ spectrum for the example planetary gear set when only FM are present due to sun gear run-out with parameters specified in Fig. 12: (a) a zoomed in view in the vicinity of the fundamental gear mesh frequency and (b) the same spectrum with a wider frequency range.

frequency modulation parameters specified above in addition to $\hat{\beta}_r = \hat{\kappa}_r = 2.0(10)^{-5}$ $(i \in [1,4])$, $\phi_{\hat{\beta}r1} = \phi_{\hat{\tau}r1} = 3\pi/2$, $\phi_{\hat{\beta}r2} = \phi_{\hat{\kappa}r2} = 0$, $\phi_{\hat{\beta}r3} = \phi_{\hat{\kappa}r3} = \pi/2$, and $\phi_{\hat{\beta}r4} = \phi_{\hat{\kappa}r4} = \pi$. The dynamic gear mesh force spectra corresponding to this case are shown in Fig. 14, which are a linear superposition of the spectra for individual errors as nonlinear behavior such as tooth separations are not in effect. The same can be said for $A(\omega)$ shown in Fig. 15 as well. Here, all of the FM sideband groups identified above for each individual error, $H_m \pm H_{p/c} \pm n$, $H_m \pm H_{r/c} \pm n$ and $H_m \pm H_{s/c} \pm n$, coexist such that each sideband can be related to a particular error since the values of $H_{p/c}$, $H_{s/c}$ and $H_{r/c}$ are distinct. It is also noted here that sideband activity due to FM is richer and more complex than that of AM sources. It can also be stated that the FM sidebands are very sensitive to parameters $\hat{\beta}_j$ and $\hat{\kappa}_j$ (j=s,r,$p1$,$p2$,…,pN), emphasizing the importance of determining their values accurately from the actual gear errors E_j using quasi-static deformable-body gear contact models.

3.2. Planetary gear set modulations near a resonance

Most of the vibration spectra measured from planetary transmissions exhibit asymmetric sidebands around the gear mesh orders. In Ref. [4], the rotation of the carrier was shown to be one of the sources of such asymmetric sidebands, unless the gear set has *equally-spaced* and *in-phase* planets as the example planetary gear set considered in this study. In agreement with this, the $A(\omega)$ spectra presented in the previous section exhibited mostly symmetric sidebands. In this

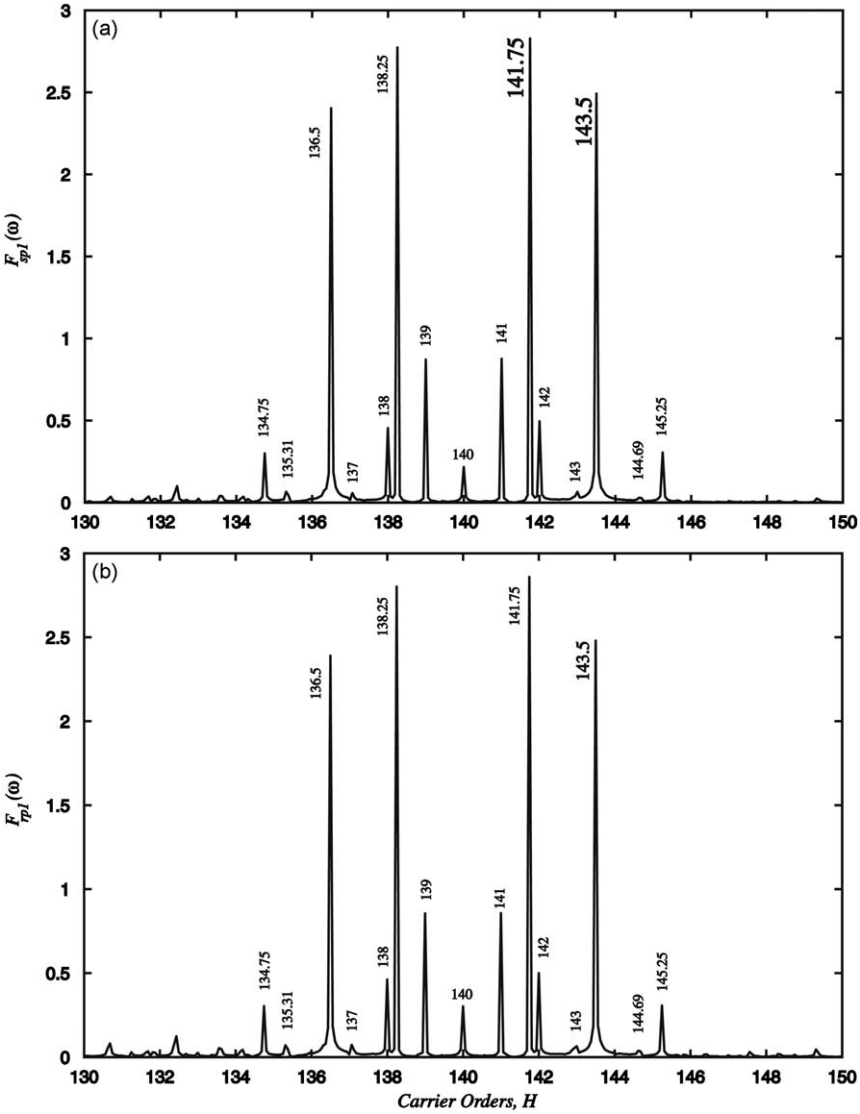

Fig. 14. Predicted (a) $F_{sp1}(\omega)$ and (b) $F_{rp1}(\omega)$ spectra for the example planetary gear set when only FM are present due to planet-1, sun gear and ring gear run-out errors. $\hat{\beta}_r = \hat{\kappa}_r = 2.0(10)^{-5}$ ($i \in [1,4]$), $\phi_{\hat{\beta}r1} = \phi_{\hat{\tau}r1} = 3\pi/2$, $\phi_{\hat{\beta}r2} = \phi_{\hat{\kappa}r2} = 0$, $\phi_{\hat{\beta}r3} = \phi_{\hat{\kappa}r3} = \pi/2$, and $\phi_{\hat{\beta}r4} = \phi_{\hat{\kappa}r4} = \pi$ and sun and planet related parameters are as in Figs. 10 and 12.

section, the sidebands of this example system will be predicted at a near-resonance region to demonstrate that dynamic effects might be attributed to some of the asymmetric sidebands as well. The steady response here is still linear (no tooth separations), partly because the damping values are not very low.

Using the same AM parameters as those used in Figs. 4 and 5 to correspond to the eccentricity of planet 1 only, the dynamic response is predicted here at a gear mesh frequency of 950 Hz that is near the natural frequency at 982 Hz. Fig. 16 shows the predicted $F_{sp1}(\omega)$ and $F_{rp1}(\omega)$ at T_s=500 N m. Here, the spectra that exhibit asymmetry about the gear mesh order H_m=140, contrasting the symmetric spectra presented in Fig. 4 for the same system at a off-resonance condition. The right-hand side sideband $H_m+H_{p/c}$=144.69 has a much larger amplitude than components at H_m and $H_m-H_{p/c}$ since this order coincides with the natural frequency at 982 Hz. Similarly, the $A(\omega)$ spectrum shown in Fig. 17 is also asymmetric about H_m for the same reason. This clearly indicates that dynamic conditions might be one of the reasons for asymmetry as well.

4. Experimental validation

These authors have recenly published a set of planetary gear set sideband modulation data collected through tightly-controlled experiments [4]. In that study, the primary aim was to validate the predictions of the proposed simplied AM

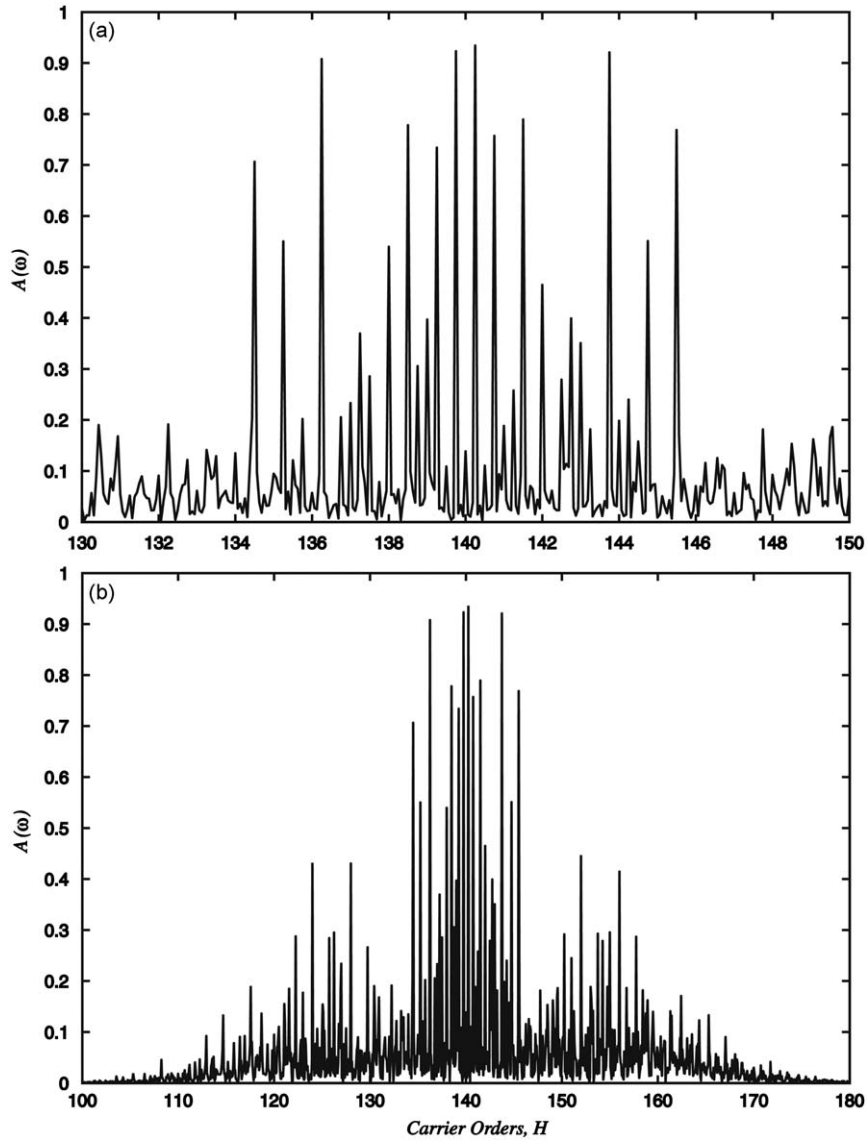

Fig. 15. Predicted $A(\omega)$ spectrum for the example planetary gear set when only FM when only FM are present due to planet-1, sun gear and ring gear run-out errors with parameters specified in Fig. 14: (a) a zoomed in view in the vicinity of the fundamental gear mesh frequency and (b) the same spectrum with a wider frequency range.

model due to carrier rotation. That model was able to describe only a subset of the measured sidebands, forming the motivation for this study. An example measured acceleration spectrum from this earlier study will be compared with the predictions of the proposed model to demonstrate the ability of the model in accounting for the gear manufacturing errors.

The planetary gear set used in the experiments had four unequally spaced planets (N=4 with ψ_i=0, 90.909°, 180° and 270.909°). For this gear set with Z_r=125, Z_s=73 and Z_p=26, an arbitrary planet phasing existed ($Z_r\psi_i$=0, 1.1325π, π and 0.1312π) such that it falls into the case (v) category in Ref. [4]. Details of the experimental set up and the experimental procedure are not included here as they can be found in Ref. [4].

Fig. 18 shows an example measured acceleration spectrum collected when this gear set was operating at T_s=400 N m and ω_s=500 rev/min. The sidebands of this spectrum at integer orders can be attributed to the amplitude modulations due to the carrier rotation. However, the sidebands appearing at orders such as 116.19, 118.19, 119.19 and 126.81 can be thought of as a direct result of certain gear manufacturing errors. These orders are associated with the planet run-out errors. The proposed model is used to simulate this gear set at the same operating condition with the AM and FM parameters associated with the run-out error of a planet gear (E_{p1}=20 μm, ε_{p1}=0). Firstly, the AM parameters corresponding to this planet gear run-out error are predicted to be β_{p1}=0.0342, $\phi_{\beta p1}$=3π/2, ϑ_{p1}=0.0335, $\phi_{\vartheta p1}$=π/2, κ_{p1}=0.0552, $\phi_{\kappa p1}$=3π/2, τ_{p1}=0.0496 and $\phi_{\tau p1}$=π/2 [26]. Predicted $A(\omega)$ spectrum is shown in Fig. 19(a) generates the measured sidebands at orders

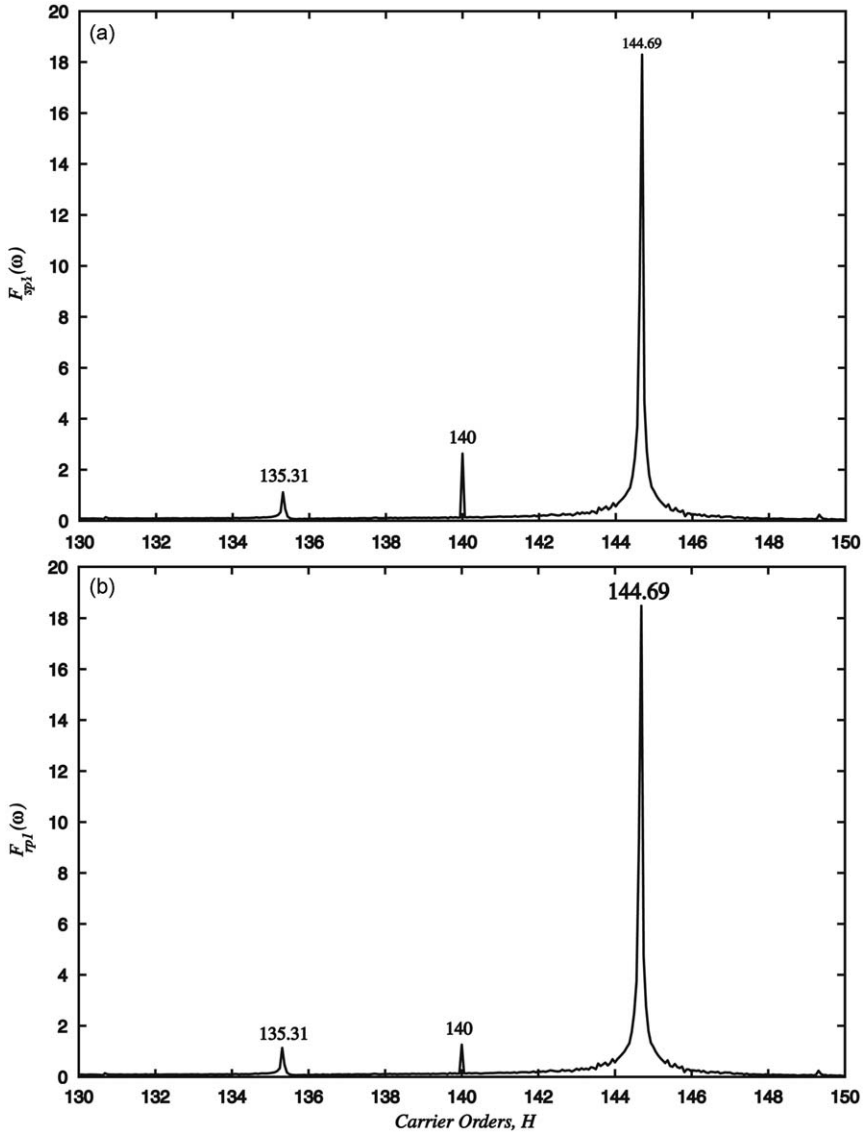

Fig. 16. Predicted (a) $F_{sp1}(\omega)$ and (b) $F_{rp1}(\omega)$ spectra for the example planetary gear set under the influence of AM due to planet-1 run-out error with β_{p1}=0.034, $\phi_{\beta p1}$=3π/2, ϑ_{p1}=0.033, $\phi_{\vartheta p1}$=π/2, κ_{p1}=0.055, $\phi_{\kappa p1}$=3π/2, τ_{p1}=0.049, $\phi_{\tau p1}$=π/2 and ω_m=151.2 rad/s.

such as 116.19, 118.19, 119.19 and 126.81 (each at $H_m \pm H_{p/c} \pm n$) in addition to even integer orders such as 120, 122 and 124 caused by the carrier rotation. Secondly, the same analysis is repeated with the corresponding FM parameters only ($\hat{\beta}_{p1} = \hat{\vartheta}_{p1} = \hat{\kappa}_{p1} = \hat{\tau}_{p1} = 1.0(10)^{-4}$, $\phi_{\hat{\beta}p1} = \phi_{\hat{\kappa}p1} = 3\pi/2$ and $\phi_{\hat{\vartheta}p1} = \phi_{\hat{\tau}p1} = \pi/2$) to produce the spectrum shown in Fig. 19(b). In this spectrum, large sideband amplitudes are evident at odd integer orders, especially at orders 123 and 127. Finally, the predicted acceleration spectrum presented in Fig. 19(c) is due to both AM and FM effects of the planet run-out error. Comparison of Fig. 19(c) to (18a) and (18b) indicates clearly that almost all of the sidebands observed in the measured spectrum are indeed predicted by the model. It further shows that the model's capability in including the gear manufacturing errors is sound. With this, it can be stated that the proposed model can be used to study sideband behavior of planetary gear sets with or without manufacturing errors in both resonance and off-resonance regions of operation.

5. Conclusions

A dynamic model was developed to predict modulation sidebands of planetary gear sets due to gear manufacturing errors in the forms of run-out or eccentricity, as well as change of the instantaneous gear mesh locations relative to a fixed

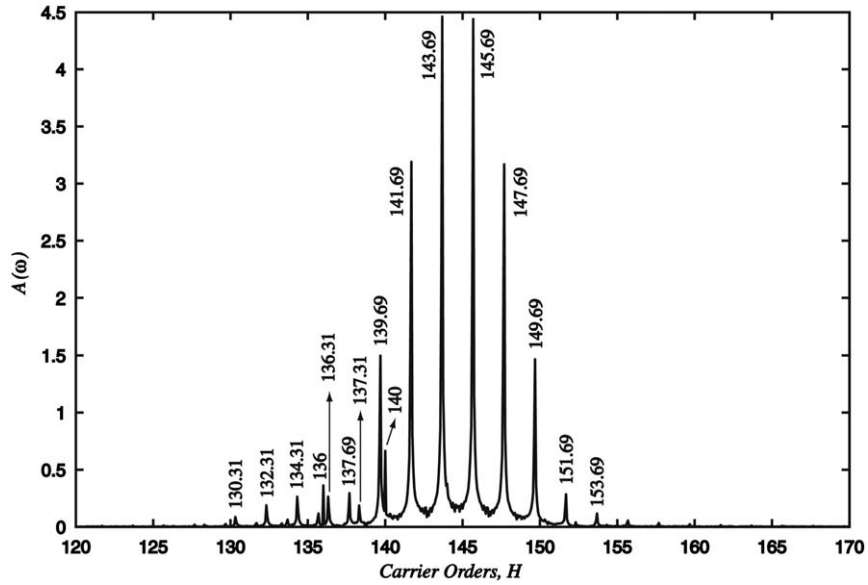

Fig. 17. Predicted $A(\omega)$ spectrum for the example planetary gear set under the influence of AM due to planet-1 run-out error with parameters specified in Fig. 16.

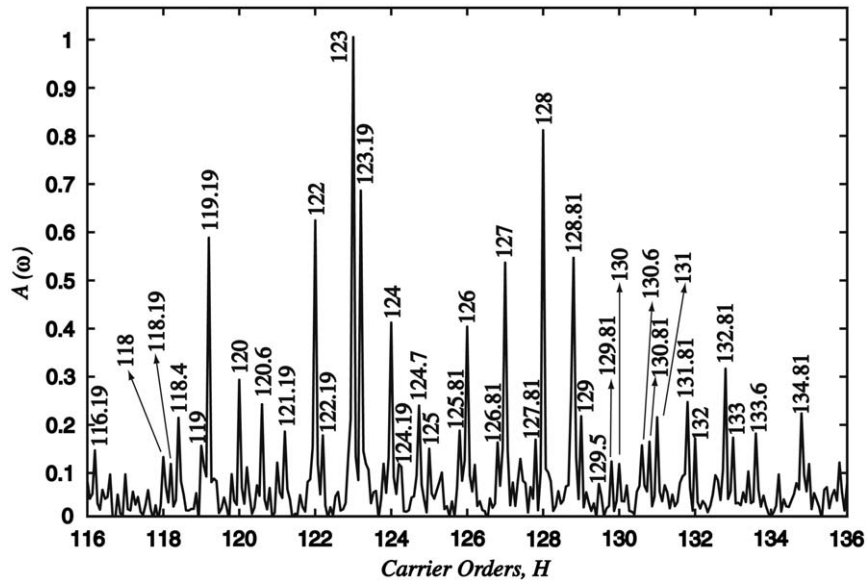

Fig. 18. A measured $A(\omega)$ spectrum from a 4-planet planetary gear set at T_s=400 N m and ω_s=500 rev/min.

measurement location due to the rotation of the planetary carrier. The dynamic model included periodically time-varying gear mesh stiffnesses and any nonlinearities associated with tooth separations. The mesh-frequency excitations were derived in their amplitude and frequency modulated forms. The resultant dynamic gear mesh force spectra were shown to contain sidebands due to these errors. These modulated dynamic gear mesh force spectra were then used in the simplified analytical formulation of Ref. [4] to include the changes caused by the rotation of the carrier. Predicted acceleration spectra were shown to contain three well-defined groups of sidebands $H_m \pm H_{p/c} \pm n$, $H_m \pm H_{r/c} \pm n$ and $H_m \pm H_{s/c} \pm n$ (n=integer) due to amplitude modulations associated with the errors of the planets, the ring gear and the sun gear, respectively, while the frequency modulations resulted in more complex sideband structures within wider frequency bands around the fundamental gear mesh frequency. At the end, comparisons to a measured planetary acceleration spectrum were provided to demonstrate that the proposed mechanisms are capable of describing the measured sideband behavior.

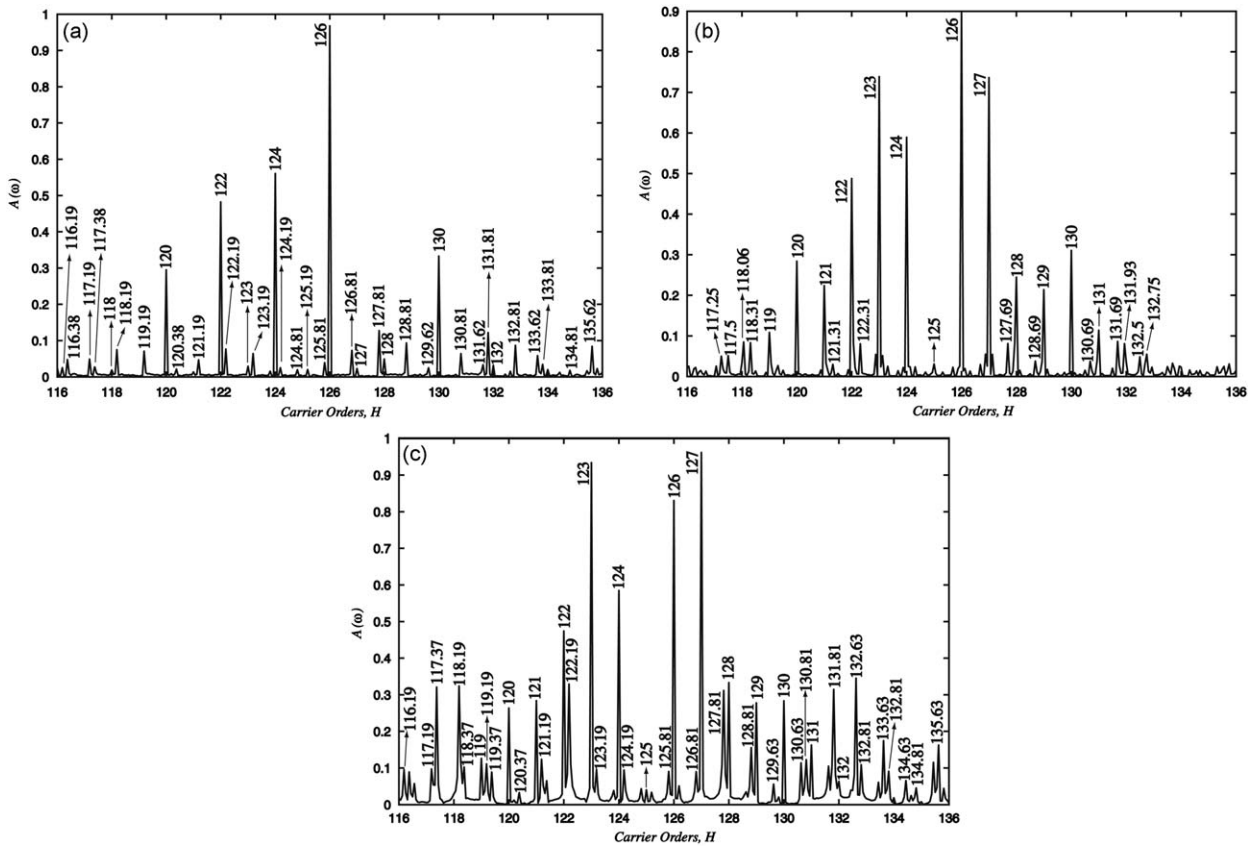

Fig. 19. Predicted $A(\omega)$ spectrum the same gear set as in Fig. 18 with (a) AM only, (b) FM only and (c) both AM and FM.

References

[1] P.D. McFadden, J.D. Smith, An explanation for the asymmetry of the modulation sidebands about the tooth meshing frequency in epicyclic gear vibration, *Proceedings of the Institution of Mechanical Engineers* 199 (C1) (1985) 65–70.

[2] P.D. McFadden, A technique for calculating the time domain averages of the vibration of the individual planet gears and the sun gear in an epicyclic gearbox, *Journal of Sound and Vibration* 144 (1) (1991) 163–172.

[3] J. McNames, Fourier series analysis of epicyclic gearbox vibration, *Journal of Vibration and Acoustics—Transactions of the ASME* 124 (2002) 150–152.

[4] M. Inalpolat, A. Kahraman, A theoretical and experimental investigation of modulation sidebands of planetary gear sets, *Journal of Sound and Vibration* 323 (2009) 677–696.

[5] A. Kahraman, G.W. Blankenship, Planet mesh phasing in epicyclic gear sets, *Proceedings of the International Gearing Conference*, Newcastle UK, September 1994, pp. 99–104.

[6] A. Kahraman, Planetary gear train dynamics, *Journal of Mechanical Design—Transactions of the ASME* 116 (1994) 713–720.

[7] F. Chaari, T. Fakhfakh, R. Hbaieb, J. Louati, M. Haddar, Influence of manufacturing errors on the dynamic behavior of planetary gears, *International Journal of Manufacturing Technology* 27 (2006) 738–746.

[8] W.D. Mark, J.A. Hines, Stationary transducer response to planetary-gear vibration excitation with non-uniform planet loading, *Mechanical Systems and Signal Processing* 23 (2008) 1366–1381.

[9] R.B. Randall, A new method of modeling gear faults, *Journal of Mechanical Design* 104 (1982) 259–267.

[10] P.J. Sweeney, R.B. Randall, Sources of gear signal modulation, *Second International Conference on Gearbox Noise, Vibration, and Diagnostics, IMechE Conference Transactions*, Vol. 5, London, England, 1995, pp. 183–198.

[11] G.W. Blankenship, R. Singh, Analytical solution for modulation sidebands associated with a class of mechanical oscillators, *Journal of Sound and Vibration* 179 (1) (1995) 13–36.

[12] A.L. Gu, R.H. Badgley, T. Chiang, Planet-pass-induced vibration in planetary reduction gears, *ASME Design Engineering Technical Conference*, New York, USA, October 1974, Paper No. 74-DET-93.

[13] A.L. Gu, R.H. Badgley, Prediction of vibration sidebands in gear meshes, *ASME Design Engineering Technical Conference*, New York, USA, October 1974, Paper No. 74-DET-95.

[14] A.M. Mitchell, F.B. Oswald, H.H. Coe, Testing of UH-60A helicopter transmission in NASA Lewis 2240 kW (3000 hp) Facility, NASA Technical Paper 2626, August 1986.

[15] M. Mosher, Results from a new separation algorithm for planetary gear system vibration measurements, *Proceedings of the ASME International Design Engineering Technical Conferences and Computers and Information in Engineering Conference*, CA, USA, September 2005, Paper No. DETC-84404.

[16] M. Mosher, Understanding vibration spectra of planetary gear systems for fault detection, *Proceedings of the ASME Design Engineering Technical Conferences*, IL, USA, September 2003, Paper No. PTG-48082.

[17] D.G. Lewicki, J.J. Coy, Vibration characteristics of OH-58A helicopter main rotor transmission, NASA Technical Paper 2705, 1987.

[18] A. Saxena, B. Wu, G. Vachtsevanos, A methodology for analyzing vibration data from planetary gear systems using complex Morlet wavelets, *2005 American Control Conference*, Portland, OR, USA, June 2005, pp. 4730–4735.

[19] D.M. Blunt, J.A. Keller, Detection of a fatigue crack in a UH-60A planet gear carrier using vibration analysis, *Mechanical Systems and Signal Processing* 20 (2006) 2095–2111.
[20] J.A. Hines, D.S. Muench, J.A. Keller, A.K. Garga, Effects of time-synchronous averaging implementations on HUMS features for UH-60A planetary carrier cracking, *American Helicopter Society 61st Annual Forum*, Grapevine, TX, USA, June 2005, Paper No. VA 22314-2538.
[21] J.A. Keller, P. Grabill, Vibration monitoring of UH-60A main transmission planetary carrier fault, *American Helicopter Society 59th Annual Forum*, Phoenix, AZ, USA, May 2003.
[22] H. Ligata, A. Kahraman, A. Singh, A closed-form planet load sharing formulation for planetary gear sets using a translational analogy, *Journal of Mechanical Design* 131 (2009) 021007-1–021007-7.
[23] A. Kahraman, H. Ligata, K. Kienzle, D.M. Zini, A kinematics and power flow analysis methodology for automatic transmission planetary gear trains, *Journal of Mechanical Design* 126 (2004) 1071–1081.
[24] M. Inalpolat, A. Kahraman, Dynamic modelling of planetary gears of automatic transmissions, *Proceedings of the Institution of Mechanical Engineers Part K: Journal of Multi-body Dynamics* 222 (2008) 229–242.
[25] W. Bartelmus, R. Zimroz, Vibration condition monitoring of planetary gearbox under varying external load, *Mechanical Systems and Signal Processing* 23 (2009) 246–257.
[26] W. Bartelmus, R. Zimroz, A new feature for monitoring the condition of gearboxes in non-stationary operation conditions, *Mechanical Systems and Signal Processing* 23 (2009) 1528–1534.
[27] A. Kahraman, Load sharing characteristics of planetary transmissions, *Mechanism and Machine Theory* 29 (8) (1994) 1151–1165.
[28] T.F. Conry, A. Seireg, A mathematical programming technique for the evaluation of load distribution and optimal modifications for gear systems, *Journal of Engineering for Industry* 95 (1973) 1115–1122.